Article, Preprint submitted to SSRN without peer review

Erosion damage progression analysis for wind turbine blade material coatings based on comparison of accelerated rain erosion testing methods and polymer properties

Fernando Sánchez *[1], Asta Sakályte[2], Mohamed Ansari[3,4], Chun-Yen Wu[5], Julie Teuwen[5], Trevor M. Young[3], Aurelio Olivares[1], Luis Domenech[1]

[1] Research Institute of Design, Innovation and Technology, University CEU Cardenal Herrera, CEU Universities, San Bartolome, 55, Alfara del Patriarca, 46115 Valencia, Spain; fernando.sanchez@uchceu.es (F.S.); luis.domenech@uchceu.es (L.D.); aurelio.olivares@uchceu.es (A.O.)
[2] AEROX Advanced Polymers, Pobla Vallbona, 46185 Valencia, Spain; asakalyte@aerox.es (A.S)
[3] Bernal Institute, School of Engineering, University of Limerick, V94 T9PX, Ireland; Mohammad.Ansari@setu.ie (M.A);
[4] Department of Aerospace and Mechanical Engineering, South East Technological University, Kilkenny Rd, Co. Carlow, R93 V960, Ireland; Trevor.Young@ul.ie (T.Y);
[5] Faculty of Aerospace Engineering, Delft University of Technology (TU Delft), The Netherlands; chunyenwu.me06@nctu.edu.tw; (C.W.); j.j.e.teuwen@tudelft.nl (J.T.);

* Correspondence: fernando.sanchez@uchceu.es (F.S.)

Received: date; Accepted: date; Published: date

Abstract:

Leading edge protection (LEP) coating systems are applied to protect wind turbine blades from rain erosion in the most critical location area. The repeated rain droplet impacts and the high speed on the blade tip are key contributors to surface erosion damage progression. The quantification of the severity of erosion in wind turbine blades is challenging due to the many aspects involved, including conditions operating, meteorology, aerodynamics, multilayer material configurations, and the blade manufacturing processes. LEP materials performance evaluation is mainly based on in-lab testing data that pretend to imitate the diverse droplet impact conditions experienced by wind turbines. This initial in-lab data durability can then be extrapolated to its in-field installation configuration for lifetime predictions and modelling estimations.

The investigation is focused in the analysis and evaluation of the erosion damage progression to link macroscopic mechanical behavior with the polymer properties and microstructure of candidate coating materials. This work scrutinises different application cases of rain erosion testing (RET), considering a comparison of the current testing standards with two whirling arm rigs and a pulsating water jet tester, in order to assess in-lab material performance for different LEP chemistries. Material characterization is supported by dynamic mechanical analysis (DMA) to observe the visco-elastic behavior of bulk coating samples. It also compares observed damage results in terms of durability aiming to extract useful data for multilayer and interfacial modeling. The damage and failure mechanisms observed are investigated using CT scanning. Variations in RET testing methods resulted in similar coating failure mode for each LEP material. Furthermore, the durability performance was ranked similarly on each testing case.

Keywords: wind turbine blades; leading edge protection; rain erosion testing; dynamic mechanical analysis; CT scan; coating characterisation

1. Introduction

Rain erosion of the leading edge of existing and newly installed wind turbine blades has seen an accelerated increase in both the onset of damage (incubation time) and the rate at which damage progresses in use. Leading edge erosion has a very significant influence on the cost of energy produced by wind turbines that incorporate new generation and therefore longer blades, following the trend in the sector. Costs include the loss of Annual Energy Production (AEP) of the wind farm due to loss of efficiency for aerodynamic reasons and the operation and maintenance costs for inspection and repair of the blades. Field repairs are expensive due to loss of availability, difficult access, work and weather conditions. It is currently the most important material technological problem due to the lack of assessment of the durability and life expectancy of wind farm installations, both new and already in operation. It affects all types of wind turbines considering onshore and offshore operators and has become a major industrial problem for the wind energy sector.

Leading edge protection (LEP) coating systems protect wind turbine blades from rain erosion in the blade tip where the repeated rain droplet impacts and the high speed are key contributors to surface erosion damage progression, see Figure 1a. Material industry solutions include liquid coatings, tapes, and shields. Although new blades use advanced materials and multilayer configuration designs, erosion affects older installations that require repair. This research focuses on post-mould liquid coatings specifically developed for Leading Edge Protection (LEP).

LEP materials performance evaluation is mainly based on in-lab testing data that pretend to imitate the rain field with the diverse droplet impact conditions experienced by wind turbines, see Figure 1b and Figure 1c. This in-lab performace durability measured data can then be extrapolated to its in-field installation configuration for lifetime predictions and modelling estimations. Validating materials for commercial use requires estimates of future behavior based on initial design properties in lab conditions. This involves required input data for the computational models to provide reliable predictions.

(a) (b) (c)

Figure 1. (a) Acquisition of inspection data for surface damage caused by blade erosion. Erosion evolves from the rotor tip to the blade root; (b) In-situ damage erosion observation for quantification and repair; (c) Rain Erosion Testing damaged sample with same material configuration after being subjected to in-lab accelerated rain field.

The quantification of the severity of erosion in wind turbine blades is challenging due to the many aspects involved, including meteorology [18][19], [9], aerodynamics [17], materials science [22][12][24] and wind turbine dynamics. All the studies are based on the required material characterization data that depends on its lab testing conditions. This initial in-lab data performance can then be extrapolated to its in-field installation configuration for lifetime modelling evaluations.

Nevertheless, other recent research [33] analyses the significant limitations of the current standard RET campaigns in accurately evaluating LEP systems for wind turbine blades. Recent advancements in viscoelastic materials pose challenges for traditional testing methods. These materials deform, dissipate energy, and recover over time, which current tests need to be configured to account for. Dynamic mechanical analysis shows that LEPs switch between elastic and brittle failure modes at a critical impact frequency. Revised testing protocols considering realistic environmental conditions are required to predict LEP performance accurately, necessitating further research.

Wear damage from raindrop impact is a fatigue process that accumulates until it reaches a set damage limit in relation with the coating layer thickness. The adhesion between layers and erosion resistance of coatings are influenced by shock waves generated by collapsing water droplets upon impact. Models predict coating lifespan and identify effective liquid-coating and coating-substrate combinations to reduce surface and interface stress developments and consecuently erosion damage.

A method to assess erosion rate can be develop with different methods. The average erosion depth over time was defined in [8]. Mass loss over time directly connected to the number of impacts, was used in [20]. There is an incubation period during which damage progresses without noticeable material weight loss. When a material reaches a critical level of fatigue degradation, it starts to lose mass at a constant erosion rate. This marks the conclusion of the incubation period and the beginning of a steady mass loss phase, during which the weight loss progresses almost linearly over time. The testing and the modelling related is recognized as the standard for quantifying damage according to ASTM G73-10 [7].

The progression of damage can be experimentally measured in laboratory conditions using various methods [23]. In this research the so-called whirling arm rig and pulsating water jets are used and compared. First, rain erosion performance is assessed using an accelerated testing technique, wherein the test material is repeatedly impacted with at high speed with water droplets in a Whirling Arm Rain Erosion Rig (WARER) in a flat specimen with a constant impact speed as described in a recent research [16]. This testing will allow us to quantify mass loss and to develop additionaly CT-Scans (due to the size of the samples), for detailed damage failure mode identification. Alternatively, rain erosion tests can be performed with the wind industry standard design used with the DNV-GL-RP-0171 [11] guideline for testing of rotor blade erosion protection systems (R&D A/S, Hinnerup, Denmark). This rig allow us tracking the erosion rate in a wide range of impact velocities that vary linearly from the tip end, which experiences the highest local velocity speed, towards the root, where the local velocity is lower. The third case of testing methodology is based on the use of pulsating water jets similarly to a recent research described in detailed in [25]. This allows to configure the droplet impact conditions to observe the material polymer viscoelastic behaviour completely.

This body of work consider two main objectives and underlying activities through the research: The first compares three liquid coating technologies formulated to provoque alternative polymer mechanical performance in the LEP configuration system; the second examines different cases of rain erosion testing considering a comparison of the current testing standards in order to asses, qualify and quantify the performance of the three material formulations.

2. Materials.

2.1 Chemistry description. Fundamental properties used in LEP cases.

Polyurethanes (PUs) are versatile materials with different properties and thus applications closely dependent on the used components. The main components for polyurethane formation are polyols, isocyanates, short chain extenders and catalysts. The structure and properties can be also changed by additives such as blowing agents, fillers, antioxidants, components containing ionic groups, etc. Typically, polyurethane materials for Leading Edge Protection are 2 component systems. Usually there is a polyol and hardener. Both components can influence mechanical performance of LEP. There are different types of polyols and isocyanates. Polyols cab be classified in 6 groups:

- Chemistry 1: Polyaspartic. Polyaspartics contain a high degree of hard segments, or high urea content, resulting in superior physical properties including optical clarity, high hardness, weather resistance, and scratch resistance. Main advantages of polyaspartics are high gloss retention during weathering, adjustable flexibility through the polyisocyanate chosen, resistance to acids and alkali, high mechanical resistance (e.g., abrasion resistance and impact strength) and ease of repair. Through the unique combination of high flexibility and hardness, polyaspartic systems can display good adhesion to the substrate and protect against atmospheric exposure, such as UV light and rain, to ensure long working lives for final material.
- Chemistry 2: Polyester polyol. Polyester-based polyurethane coatings show enhanced UV resistance, excellent resistance to oils and fuels, and better abrasion resistance and tensile and tear strength compared to polyether-based polyurethane coatings. However, polyester-based polyurethane coatings are more susceptible to hydrolysis and provide poor resistance to weak acids and bases compared to polyether-based polyurethane coatings.
- Chemistry 3: Polyether polyol. Polyether-based polyurethane coatings exhibit enhanced hydrolytic stability and excellent resistance to weak acids and bases compared to polyester-based polyurethane coatings. However, polyether-based polyurethane coatings are more susceptible to UV radiation and provide poor resistance to oils and fuels compared to polyester-based polyurethane coatings.
- Chemistry 4: Polyether-polyester polyol. As seen in sections above, polyester and polyether polyurethanes have unique characteristics that make them suitable for different applications. Polyether-polyester polyols can combine the main properties of both chemistries, such as hydrolytic stability and durability of polyethers and abrasion and UV resistance of polyesters.
- Chemistry 5: Polycaprolactone polyol. Higher performance polyesters such as polycaprolactones are formed by ring opening of a heterocycle ring (caprolactone monomer) by a glycol initiator. The nature of this reaction results in a low polydispersity. Consequently, polycaprolactones have significantly reduced viscosities, enhanced mechanical properties, as well as enhanced low temperature and high temperature performance properties. The properties of polycaprolactone diols for UV resistance and heat resistance is better than polyether diols. In addition, polycaprolactone diols also have better property for hydrolysis resistance than adipate based polyester diols.
- Chemistry 6: Polycarbonate polyol. Polycarbonate diols easily reacts with isocyanate compounds and generates polymers with characteristic such as durability and chemical/hydrolysis resistance. Compared to standard polyester polyols, polycarbonate diols provide significantly enhanced hydrolytic stability, impact resistance, flexibility, and chemical resistance. Polycarbonate-polyurethanes enhanced UV resistance, excellent resistance to oils and fuels, and better abrasion resistance and tensile and tear strength compared to polyether-based polyurethanes.

The PU structure depends on the relative ratios of the main compounds. Due to those wide possibilities, polyurethanes can be obtained in the form of rigid or flexible foams, thermoplastics, CASE (coatings, adhesives, sealants and elastomers) and waterborne dispersions [34]. Polyurethane coatings are particularly recommended for application to surfaces subject to high levels of wear-and-tear, because they combine outstanding resistance to solvents and chemicals with good weather stability and they exhibit very good mechanical properties and provide the ideal balance of hardness and flexibility, even at low temperatures [35].

Polyurtehane mechanical properties can be tuned by selecting different polyol or different isocyanate [35]. Polyurethane properties can be tailored by changing the composition: either by means of substrates or varying the molar ratio of the components. Moreover, PU properties strongly depend on the crosslinking of the polymer chains and it can be modified by the crosslink density. The strength of polyurethane is ensured by its specific molecular structure, which is highly resistant to mechanical stress. The molecular bonds in a polymer give it strength and the ability to withstand

significant loads without deformation or destruction. This makes polyurethane an ideal material for use in intensive environments where a high degree of reliability and durability is required.

Three different formulations were adressed for this research. The material fundamental properties of the coatings are presented in **Table 1** with the bulk materials of PA, PB and PC.

Table 1 Fundamental material and mechanical properties of the LEP systems of the study

Coating Polymer Reference	Density Part A (g/cm3)	Pull-off (MPa)	Speed of Sound (m/s)	Elastic Modulus (MPa)	Ultimate Tensile Stress (MPa)
PA	1,124	5,95	1807,00	7,00	2,69
PB	1,092	5,79	1627,00	5,00	1,33
PC	-	Failure to achieve proper adhesion	1710,00	1,00	2,11

2.2 Material. Viscoelastic characterization. Dynamic mechanical analysis.

Recent coating technologies aimed at preventing erosion utilise viscoelastic materials. These coatings exhibit high-rate transient pressure build-up followed by relaxation across various strain rates. In order to analyze the erosion performance appropriate characterization for such viscoelastic materials is then required and represents one of the main objective of this work to avoid lack of completeness. A modelling methodology that allows one to evaluate the frequency dependent strain-stress behavior of the multilayer coating system under single droplet impingement was presented in [12]. Other recent works have been focussed in rain erosion testing impact conditions [1].

Dynamic Mechanical Analysis (DMA) testing was explored as a means to get a quantification of the mechanical properties of the coating materials. Some of the findings were published in [1]. (DMA) tests were performed to characterize the material and observe the visco-elastic behavior of bulk PU samples. Several type of DMA test fixtures are available, for testing coatings, typically tensile clamps are considered the most suitable, due to the small thickness of the bulk PU samples [2]. In the tests, a static and dynamic load can be set and both frequency and/or temperature scans can be performed.

To establish the full visco-elastic behaviour, both frequency and temperature scans are required to construct the mechanical properties over a full range through time-temperature-superposition (for instance William Landel Ferrel, WLF). This is important as the frequency of impact has a large effect on the mechanical properties of the coating – where higher frequencies typically results in more elastic behaviour, and lower frequencies in more viscous behaviour. The extrapolation of the frequency scans to higher frequencies will be more accurate when temperature scans at different frequencies have been performed as well. The test results from the DMA include: storage modulus (elastic behaviour of the material), loss modulus (viscous behaviour of the material). From the data, the tan(delta) which is the loss modulus divided by the elastic modulus, and the glass transition temperature (transition between glassy and rubbery state of a material) can be derived [3]. It is has been hypothesised that the higher the tan(delta) for a given coating materials at the frequency of impact (range 10^4-10^7) the better the LEE erosion behaviour. Frequency sweeps in the DMA are typically in the order of 10^(-6)-10^(2) Hz [4], therefore the time-temperature superposition is needed in the analysis. This relies on the fact that behaviour at lower temperatures corresponds to behaviour expected at higher frequencies, and their relation is dependent on a shift factor, as outlined by WLF.

The storage modulus and loss modulus were measured experimentally as a function of temperature from a DMA test at a constant frequency. Using the time-temperature superposition (TTS) principle, the data at different temperatures were horizontally shifted along the temperature axis to overlap with a reference temperature creating a smooth and continuous master curve in the

frequency domain. The shift factor quantifies the amount of horizontal shifting required at each temperature and is typically described by empirical models such as the Williams-Landel-Ferry (WLF) equation or the Arrhenius equation, depending on the material's behaviour [5]. This approach allows the consolidation of temperature-dependent viscoelastic data into a single master curve, effectively extending the material's response over a broader range of equivalent frequencies or time scales. The resulting master curve provides insights into the material's thermorheological behaviour and its dependence on temperature and time. In this study the WLF equation was used with already known universal constants for amorphous polymers [5]. These constants are assumed as valid for most polymers when the reference temperature at which the polymer is studied coincides with its glass transition temperature. However, if the reference temperature differs from the glass transition temperature, these constants change and must be adapted consequently. The documentation of the finite element software ABAQUS provides a methodology to estimate these new constants at another reference temperature based on the original universal constants and the difference between the reference temperature and the glass transition temperature [6].

The results were obtained for 1 temperature sweep at 1Hz, are shown in Figure 2. At high impact velocities (and therefore frequencies, range 10^4-10^7) the behaviour of PA and PB is similar (as can be explained by the similar tan(δ) at low temperatures) meanwhile the PC is considerably higher. Relating LEE erosion data with DMA data within the scope of this research is discussed in next sections.

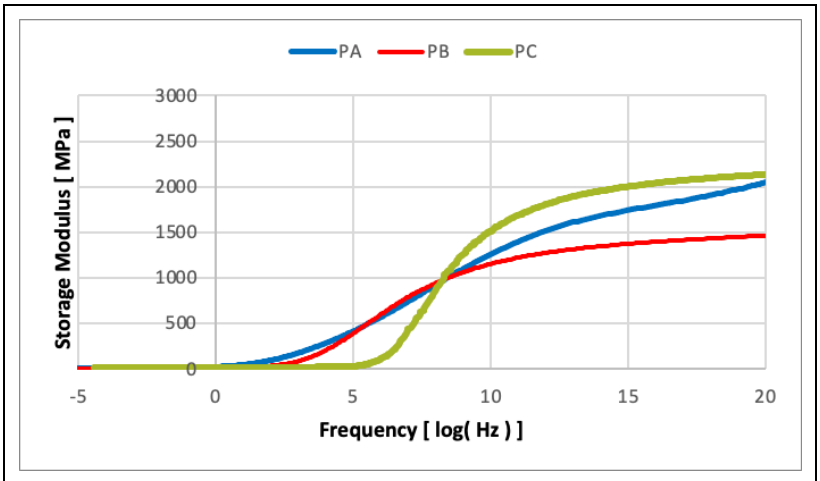

a)

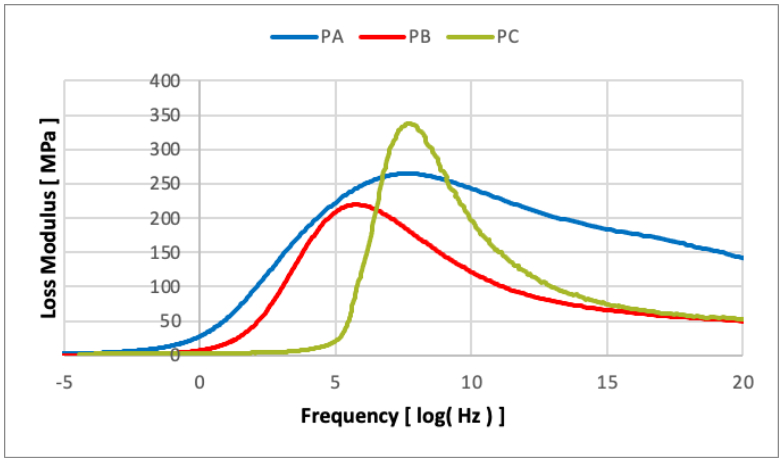

b)

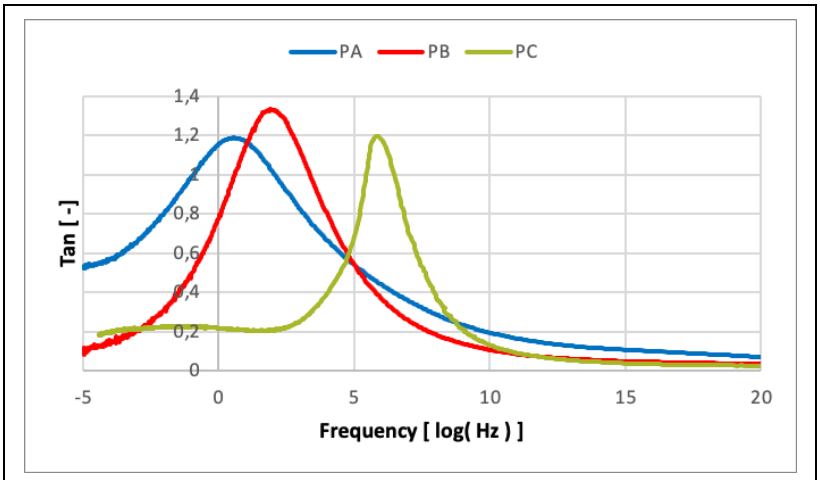

c)

Figure 2. Viscoelastic characterization from the DMA master curves and the time-temperature superposition analysis of the three coating materials of this study.

2.3 Interface characterization. Peeling adhesion testing

Erosion damage from rain droplets is typically analyzed as direct impact on a rigid surface, but it actually involves dynamic shock wave propagation. As the water droplet impinges on the surface at a normal angle, two wave fronts are created with the longitudinal compressional normal stress wave preceding a transverse shear wave. The impact gives rise to a third wave due to the water droplet deformation itself, called the Rayleigh wave, which is confined to the surface of the target and contains important amount of the collision energy. The post-impact shock wave also propagates through the multi-layer system materials and depends on the elastic and viscoelastic responses, the surface preparation, coating application and the interactions between layers [37][38]. This impact shock wave is also reflected wherever the acoustic impedance properties differ locally, so microstructural defects, such as voids, blisters and lack of adhesion, play a key role on the degradation of a particular coating. Hence, indirect damage by delamination may occur at the interface boundaries between material layers, caused by the propagation and interaction of the compressional waves from the impact of water droplets, as shown in Figure 3. The erosion failure can be initiated by a local imbalance of tensile and shear stresses in regions that may be outside the direct impact area through the thickness [36].

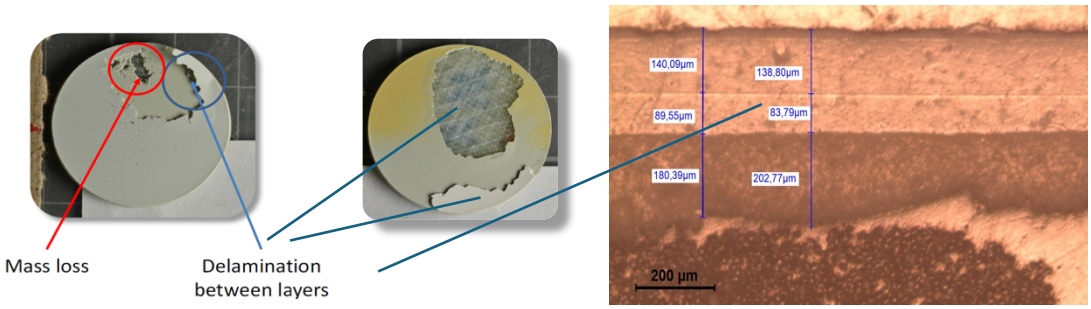

(**a**) (**b**)

Figure 3. (**a**) Two different types of erosion failure: pits and cracks that progress with mass loss caused by direct impact and stress on surface (left) and delamination indirectly caused by the interface stresses (right). (**b**) Cross section of a multi-layered system. Two consecutive coating layers and coating–substrate interfaces in which delamination tend to appear upon impingement.

The coating's ability to transfer wave energy within a multi-layered system impacts erosion damage. Stress reflections oscillate through the coating and substrate until dampened by the materials, reducing the initial shockwave energy. Post-mould coatings are commonly developed for Leading Edge Protection (LEP), where the impact energy from rain droplets is significantly higher due to increased tip speeds. These LEP elastomer material coatings are engineered with a low macroscopic elastic modulus, high ultimate strain, and high resilience to reduce stress at the impact surface and dampen stress waves depending on its viscoelastic response. The material recovers quickly and dissipates energy efficiently based on its dynamic properties and thickness. These materials store energy at low stress levels but require proper adhesion between the coating and substrate. To lower total free energy, pits and micro-cracking occur as a recovery mechanism. Damage progresses on the surface usually with surface pits and cracks, causing mass loss and following fatigue characteristics. Intermediate layers of putty fillers may develop complex stress wave interactions. Improving interface adhesion helps reduce delamination, thereby increasing the system's durability under repeated impacts.

The typical mechanical testing used in the wind turbine industry for material qualification is developed in order to assess the macroscopic behaviour of the multilayer configuration adhesion. In Table 1 of the previous section, pull-off strength testing of the samples shows different values. Since Pa and PB have similar results and adhesive failure, the PC shows cohesive failure in which the failure is in the composite laminate and hence the ability of the coating to assure the required target strength. Additionally, developed peeling testing for interphase coating-filler adhesion response quantification shows that PA and PB have poor values of the energy release rate and adhesive failure, meanwhile PC shows partially cohesive failure noting improved interphase capabilitites.

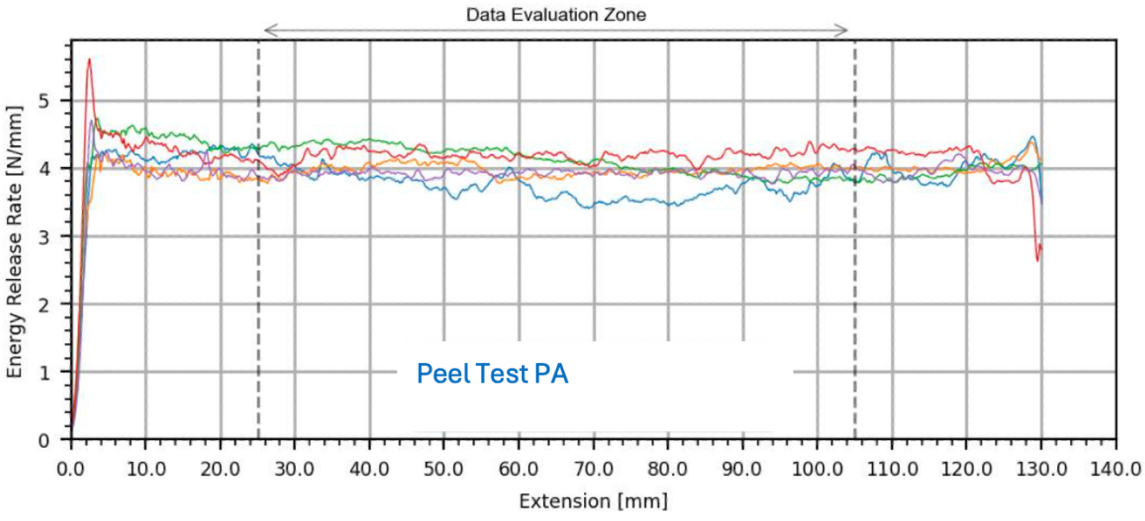

a)

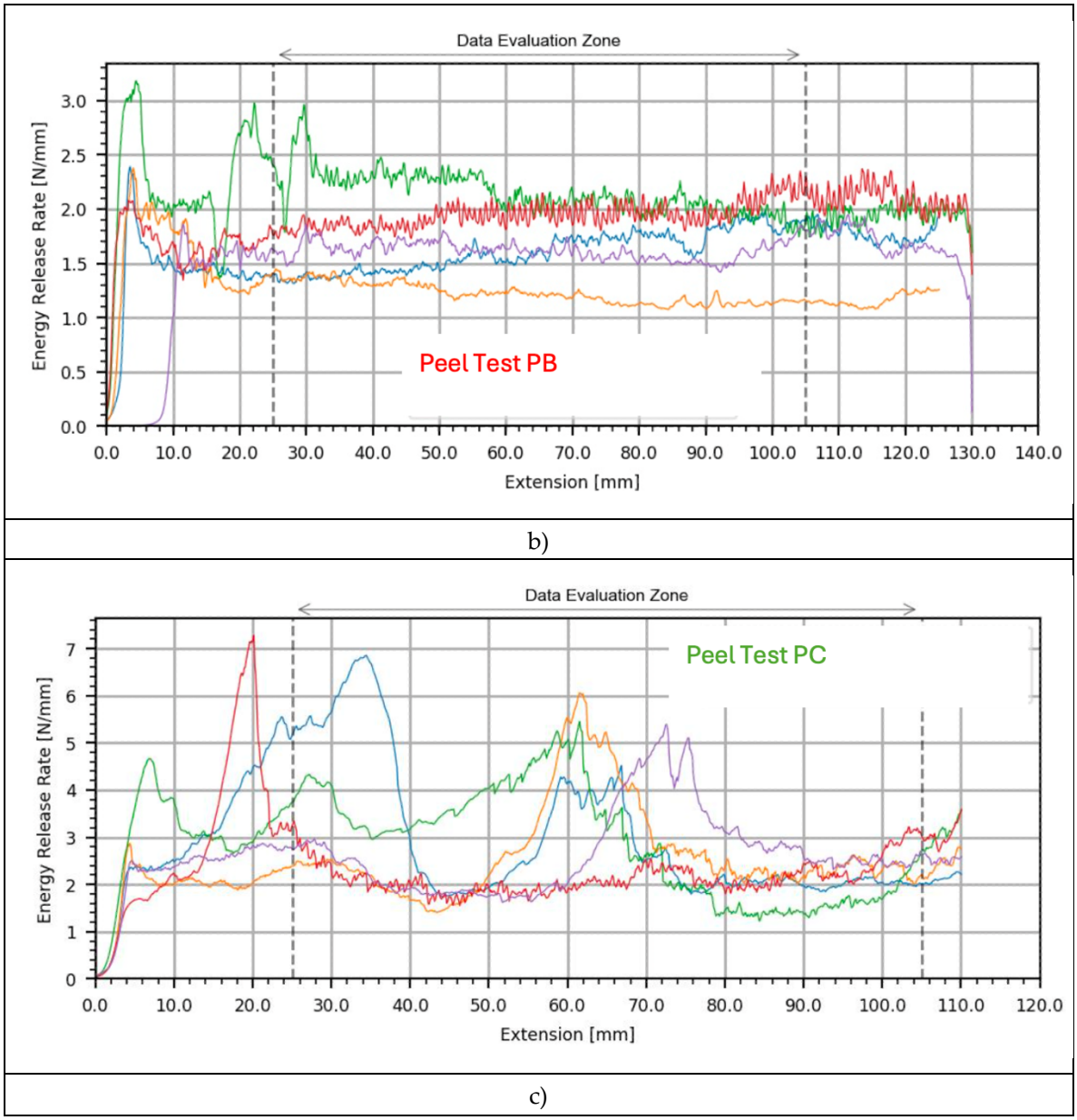

Figure 4. . Interphase adhesion peeling testing (a) Coaing PA; (b) Coaing PB; (c) Coaing PC.

3 LEP performance comparison in rain erosion testing. Results and discussion.

3.1 Case 1. Rain Erosion Testing Rig based on ASTM G73-10 performed in WARER, University of Limerick

The whirling arm method uses a sample on an arm, rotating through artificial rain from nozzles or needles [23]. Despite its simplicity, various designs exist, differing in rain-field generation, and sample number, size, and shape.

In this research case, rain erosion testing is performed in WARER at the University of Limerick as shown Figure 5. The standard used (ASTM G73 – 10: Standard Test Method for Liquid Impingement Erosion Using Rotating Apparatus) is an old standard for testing liquid impingement erosion. It covers both random and single-point droplet impacts, focusing on the incubation period of a coating. The standard uses total impingement and specific impacts to compare results between different setups.

The WARER is equipped with 36 blunt needles around its perimeter and one rotating arm. The blunt needle has a diameter of 2 mm and a rainfall rate of approximately 25 mm/h. The coupons were tested at 135 m/s. Before testing, the test sample is dried overnight in an oven as indicated Figure 6(b) following water jet cutting. The whirling arm rotates at a rate of 2154 revolutions per minute. As heat is generated inside the chamber a chiller is used to maintain the temperature inside the chamber to a nominal 16°C. The test coupon is inserted into the coupon holder at one end of the rotating arm, as shown in Figure 6(d). Time interval of 15 minutes is taken for the fatigue testing and mass loss is captured during the test. 3 specimens were tested for each configuration and water jet is used to cut the coupons with 27mm disc diameter and dried at 45 ^{0}C to ensure the coupons are moisture free before testing. Afterwards, the specimens were exposed to RET and the specimens were removed from the chamber in regular intervals and the same process and measurements were repeated (specimens were dried, weighed and photographed).

The rain erosion tests where develop for the three coating cases with the LEP configuration shown in Figure 7. It can be observed in Figure 8 the damage progresion for the three coatings PA, PB and PC. In all the cases is observed how the erosion failure advances from the surface through the multilayer system thickness until it reaches the composite laminate. The incubation time (start of perceptible erosion) is outlined through the mass loss evolution depicted in Figure 9 and can be determined similarly in the pictures. Results shows that the material PC offers better durability in terms of erosion resistance than PB and the worst PA. In regards the failure damage progresion, it is observed that delamination occurs only in the first and second configurations, PA and PB, but not PC. This is coherent with the increase in fracture energy revealed by the peeling testing values. Adhitional CT-Scans where developped for the coating tested samples at the end of the testing to analyse thorugh the thickness the failure modes. Results shown in Figure 10, Figure 11, and Figure 12, confirm the improved adhesion capability of PC and delamination failures at coating-filler interfacefor PA and PB. Nevertheless, it is also observed that PA reached also delamination at filler-laminate one, probably because of the excess on testing time and complete sample degradation.

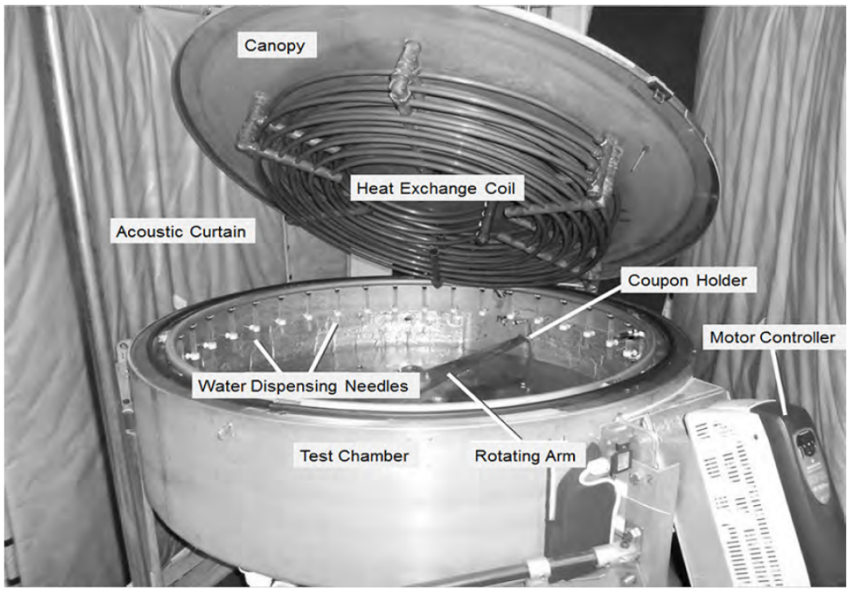

Figure 5. Whirling Arm Rain Erosion Rig (WARER) at University of Limerick from (O'Carroll et al.,2018)

(a) (b) (c) (d)

340 **Figure 6.** Rain erosion a) whirling arm rain erosion rig (WARER) at University of Limerick b)
341 oven c) chiller d) coupon holder

342

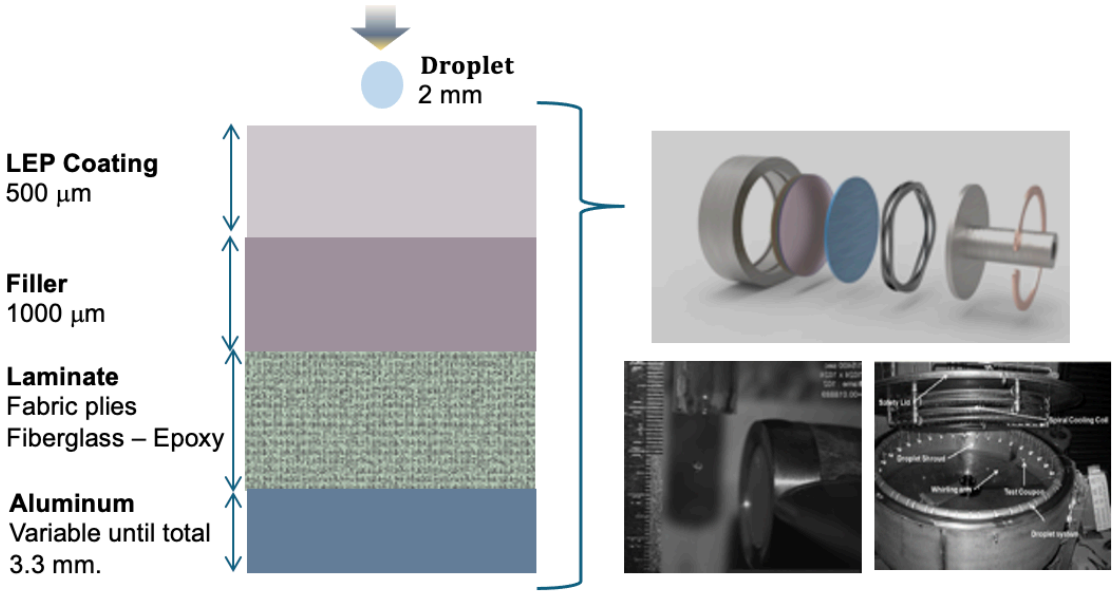

343

344 **Figure 7.** Test specimen multilayer configuration

345

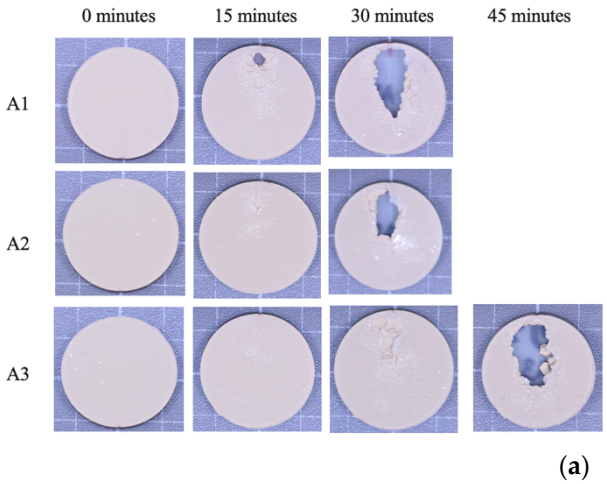

(**a**)

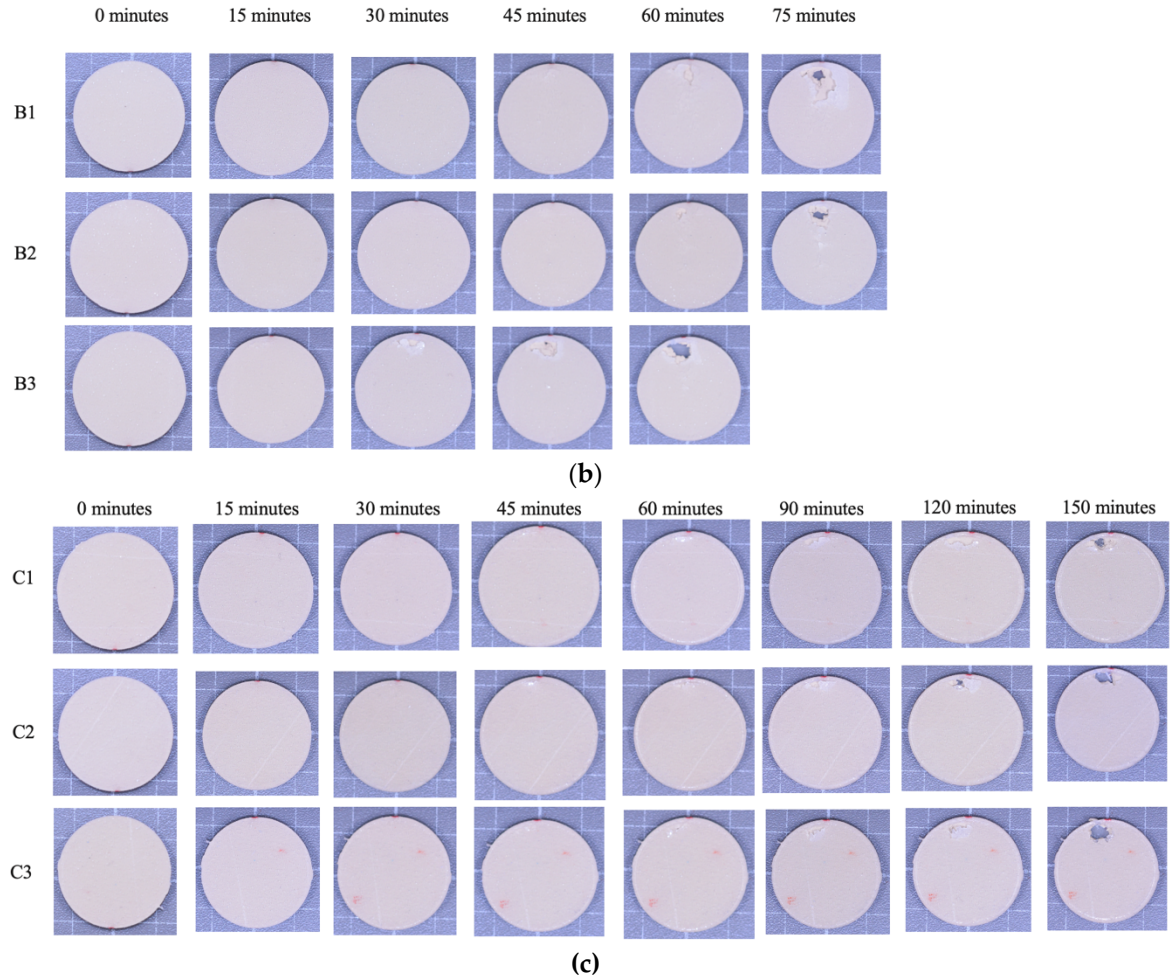

346 **Figure 8.** Damage progresion on the test samples for materials A, B and C after 45, 75 and 150
347 min testing.

348

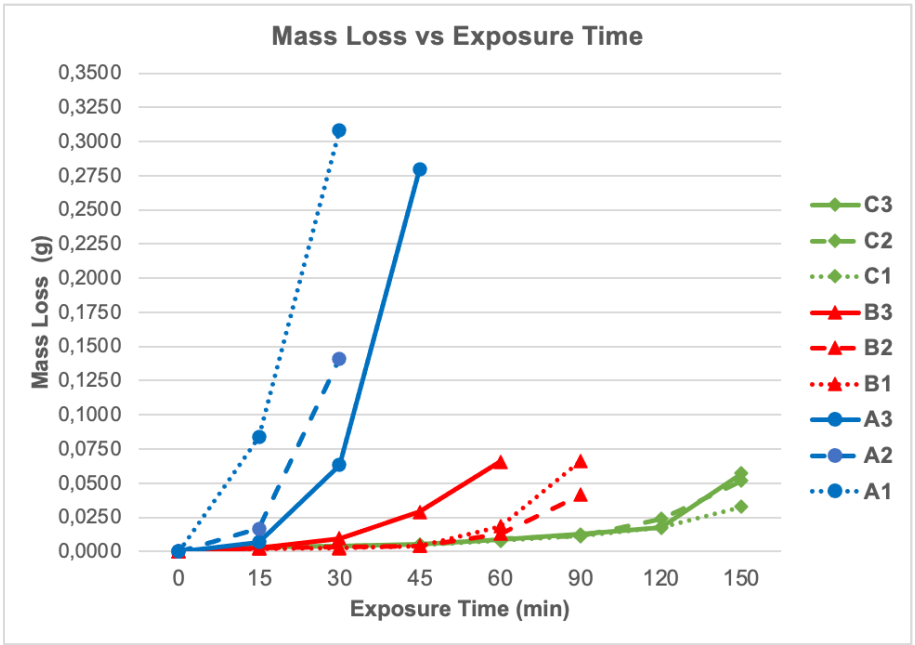

349
350 **Figure 9.** Mass Loss evolution for the two tested LEP materials

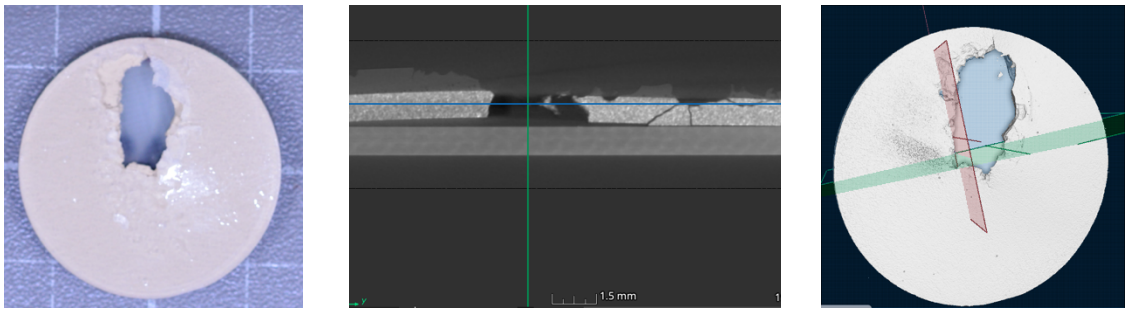

A2, 45 min
(a) (b) (c)

Figure 10. Representative specimen of Polymer PA, sample A2, after 45 min testing (a) picture, (b) microCT and (c) view analysis description. Delamination damage observed at LEP-Filler and Filler Laminate interfaces.

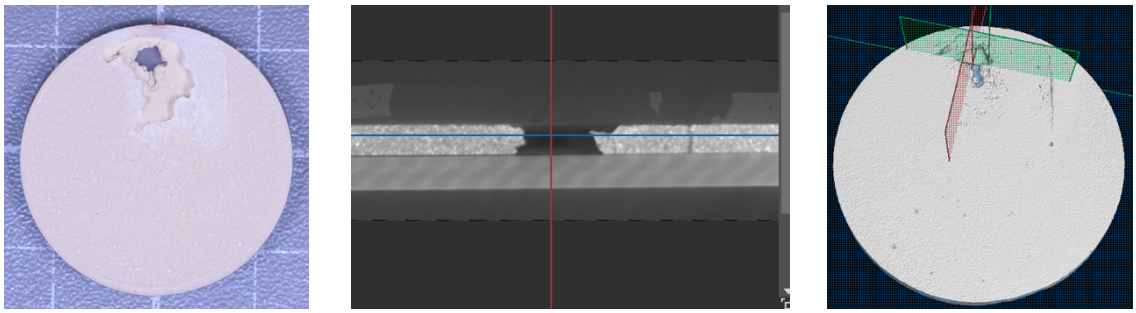

B1, 75 min
(a) (b) (c)

Figure 11. Representative specimen of Polymer PB, sample B1, after 75 min testing (a) picture, (b) microCT and (c) view analysis description. Delamination damage observed at LEP-Filler and Filler Laminate interfaces.

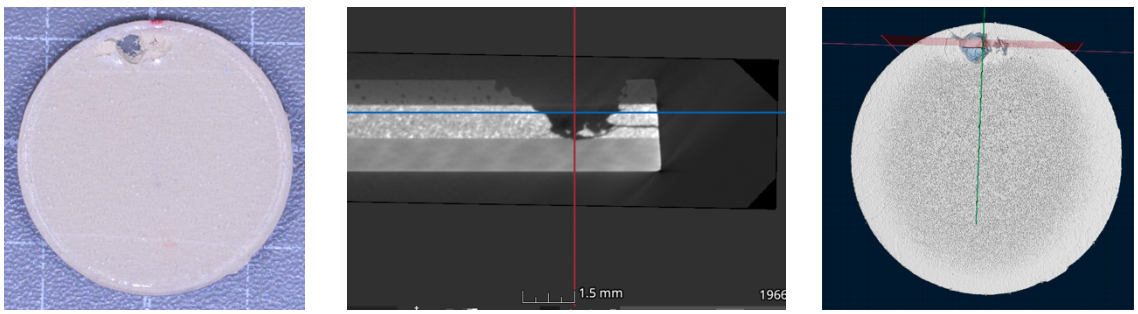

C1, 150 min
(a) (b) (c)

Figure 12. Representative specimen of Polymer PC, sample C1, after 150 min testing (a) picture, (b) microCT and (c) view analysis description. Wear damage observed at LEP and Filler but no delamination at interfaces.

These results of erosion durability of the rain erosion tests, correlate well with the viscoelastic response depicted in Figure 2 based on DMA testing. Coating PC shows best erosion performance at the high speed testing of 135 m/s due to its improved capabilitites of attenuating energy at high frequency values in the range of (10^4-10^7). The incubation time is delayed and also decreased the erosion rate. Lower performance are achieved by PB and PA due to their limited high frequency response. Nevertheless, it is important to note that the testing developped in this rig accounts only for a constant speed so conclusions may be different when considering lower impact speed values at testing as will be remarked in next sections. In regards the observed delamination as the root cause of erosion, it is not possible to conclude it since the adhesion values can not be related now with the viscoelastic response, so additional testing should be completed.

3.2 Case 2. Rain Erosion Testing Rig based on DNVGL-RP-0171

This section describes the testing results used to examine the erosion resistance and durability of the three PA, PB and PC coatings. It outlines the test plan considering the whirling arm rain erosion testing based on DNVGL-RP-0171 [11]. This testing is most used by industry to qualify materials and for the evaluation of in-field erosion performace with DNVGL-RP-0573 [10].

The DNVGL-RP-0171 [11] modifies ASTM G73-10 [7] testing and data analysis to fit the new tester developed by R&D A/S. While ASTM G73-10 [7] uses small rotating test coupons in a uniform rain field, see Figure 5 in previous section, the R&D A/S tester used in [32], see Figure 13, employs a diverging rain field with long curved blade samples, see sample configuration used in Figure 14. This results in a radial speed variation and rain intensity gradient in the tester as detailed and explained in DNVGL-RP-0171 [11]. Incubation detection requires optical methods to track erosion damage due to design differences, rather than using mass loss data.

Testing results are shown visually in Figure 15, Figure 16 and Figure 17, for the three coating cases. The erosion damage progression analysis is quantified and reported with the the data obtained in Figure 18 with the plotted V-N curves and their fitting curves with linear regression for the three cases of the analysis. In Figure 19 the equivalent data is also plotted offering the exposure time values instead of the number of impacts.

Figure 13. Rain Erosion Test developed in Aeronordic, from [32].

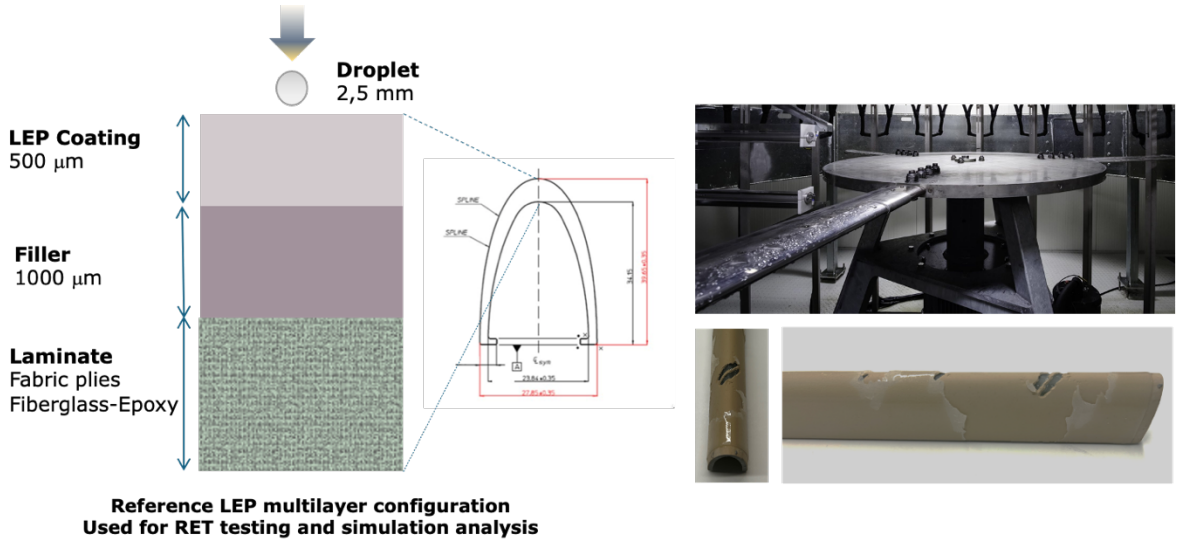

Figure 14. Testing samples configuration used in RET testing based on DNVGL-RP-0171 [11] for the three coating cases PA, PB and PC.

Exposure Time	PA
00:00	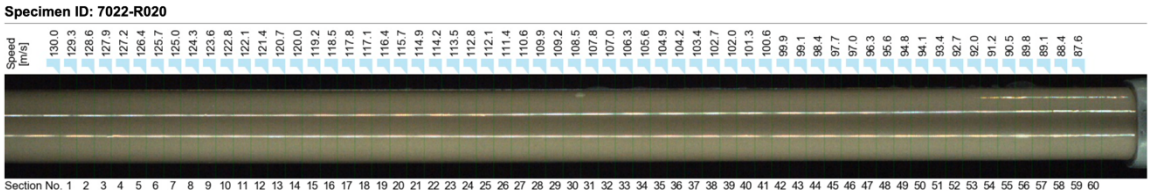
01:00	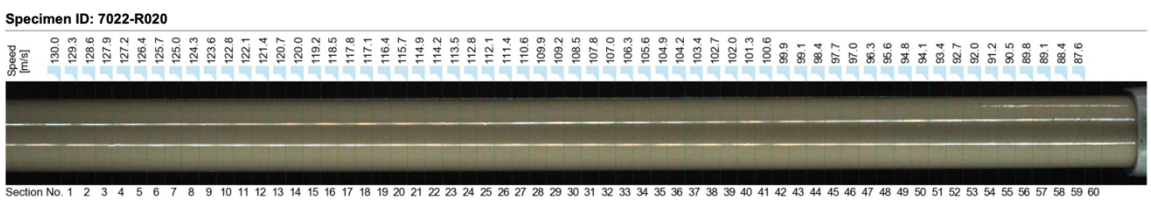
01:40	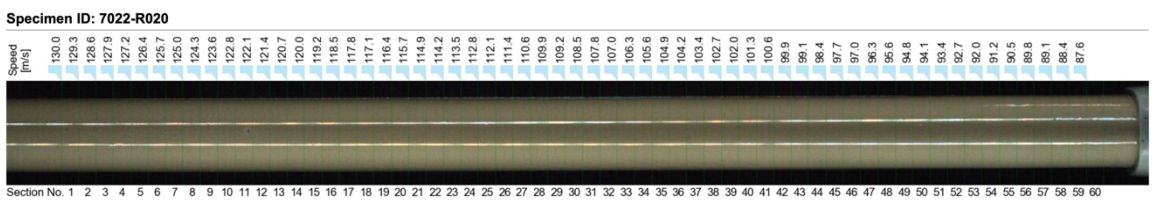
02:00	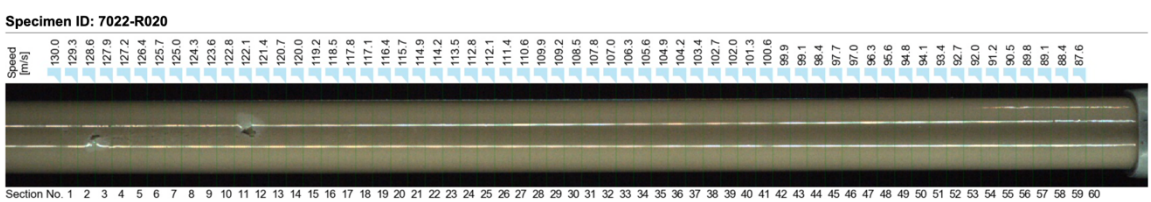

02:20	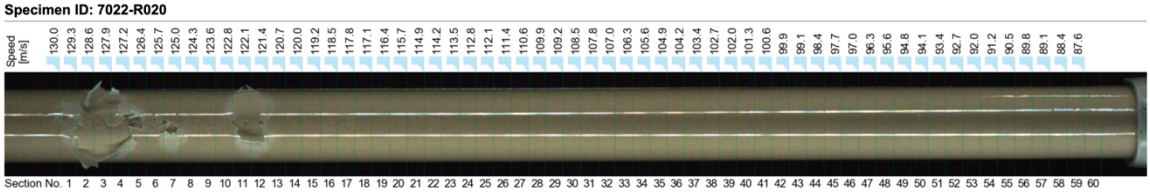
02:40	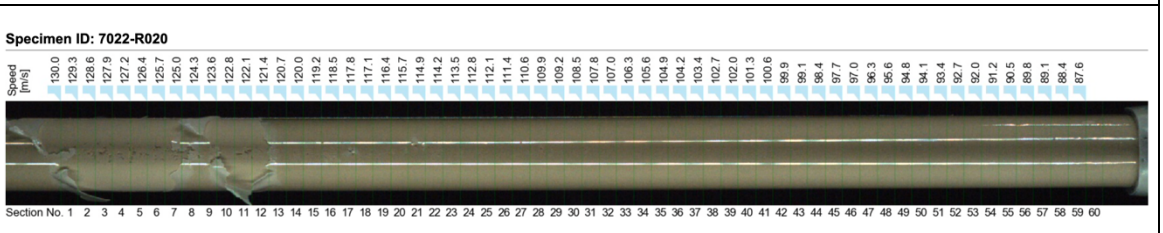
3:00	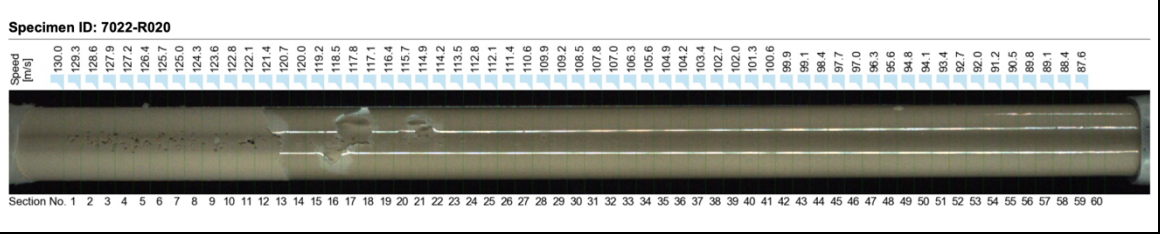

Figure 15. RET testing case for PA with images captured at different time intervals.

Exposure Time	PB
00:00	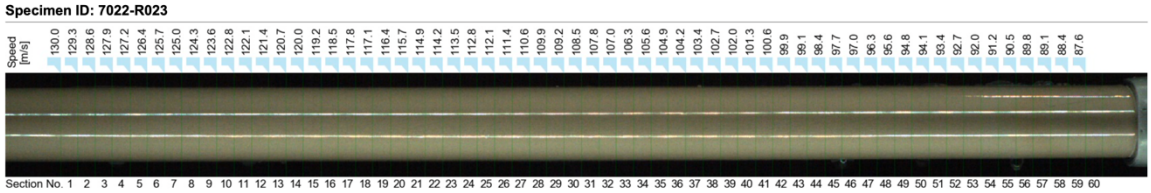
9:00	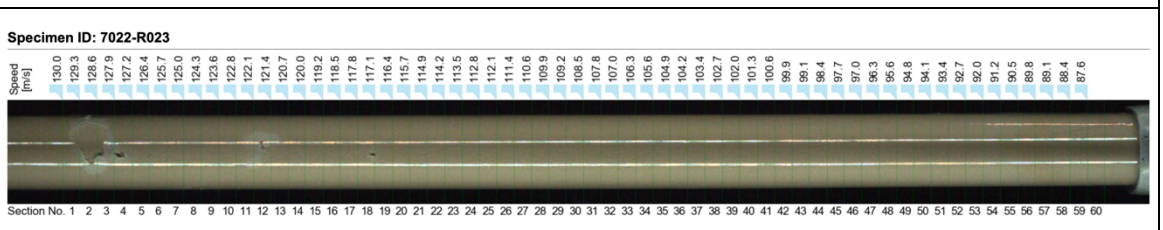
10:00	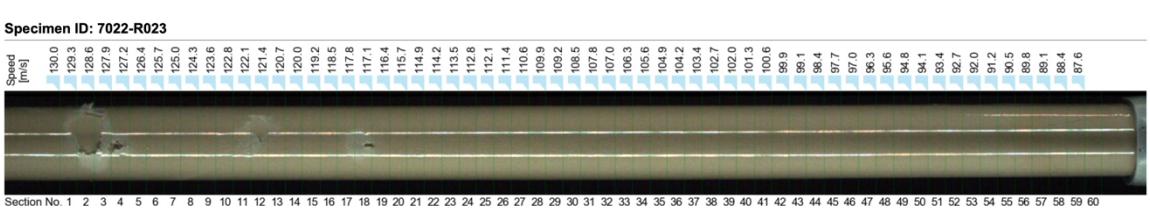
11:00	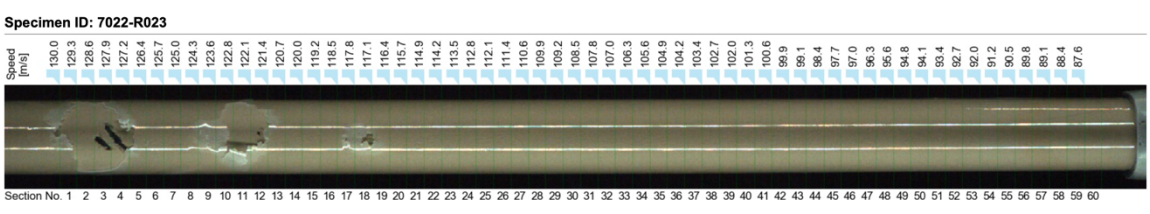

11:20	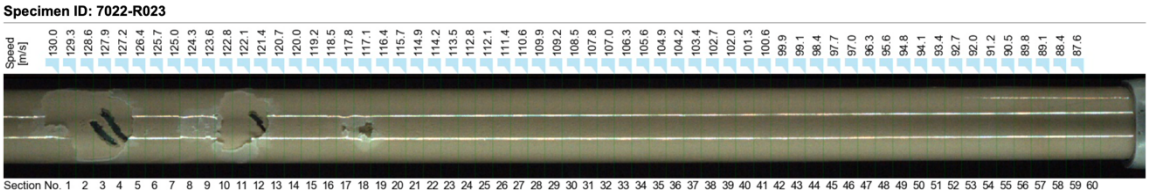
11:40	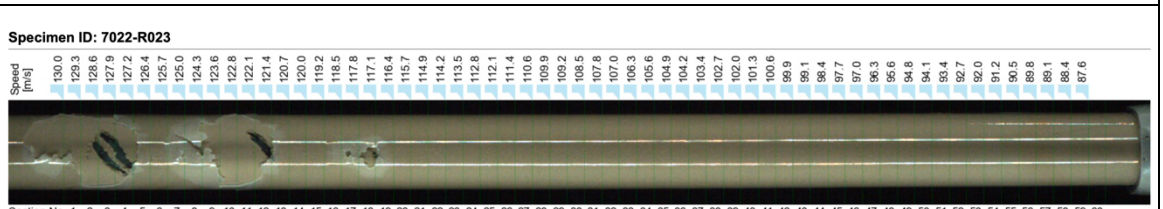
12:00	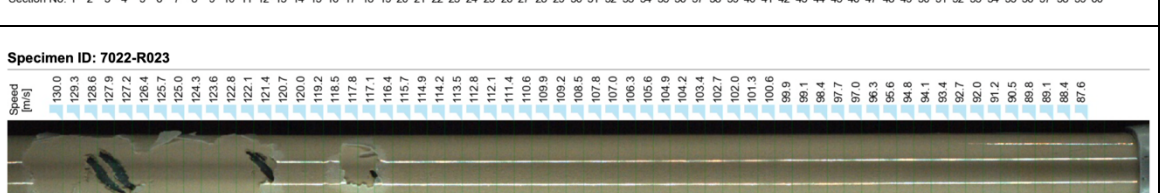

Figure 16. RET testing case for PB with images captured at different time intervals.

Exposure Time	PC
00:00	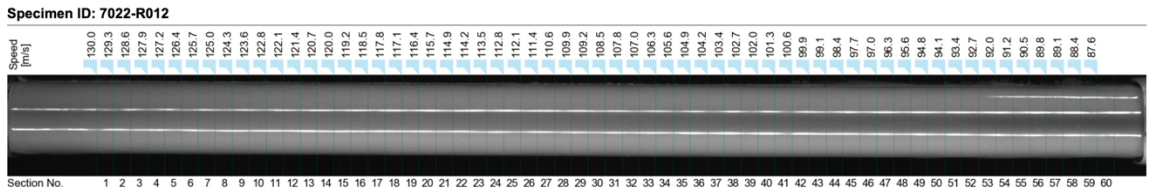
13:00	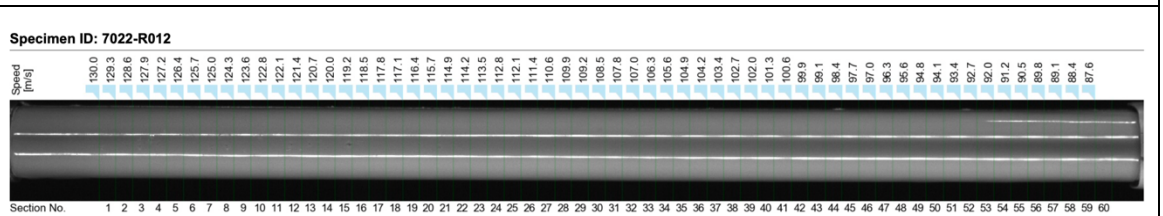
14:00	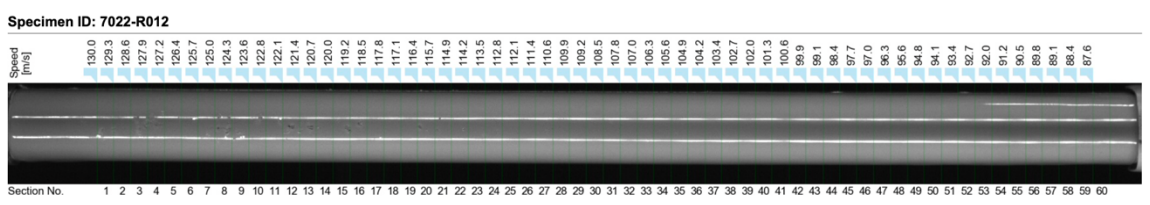
15:00	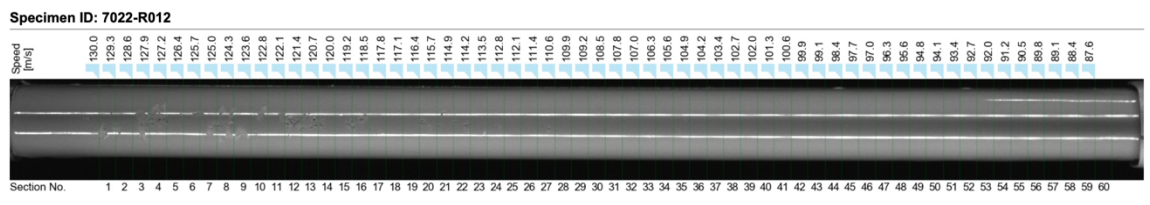

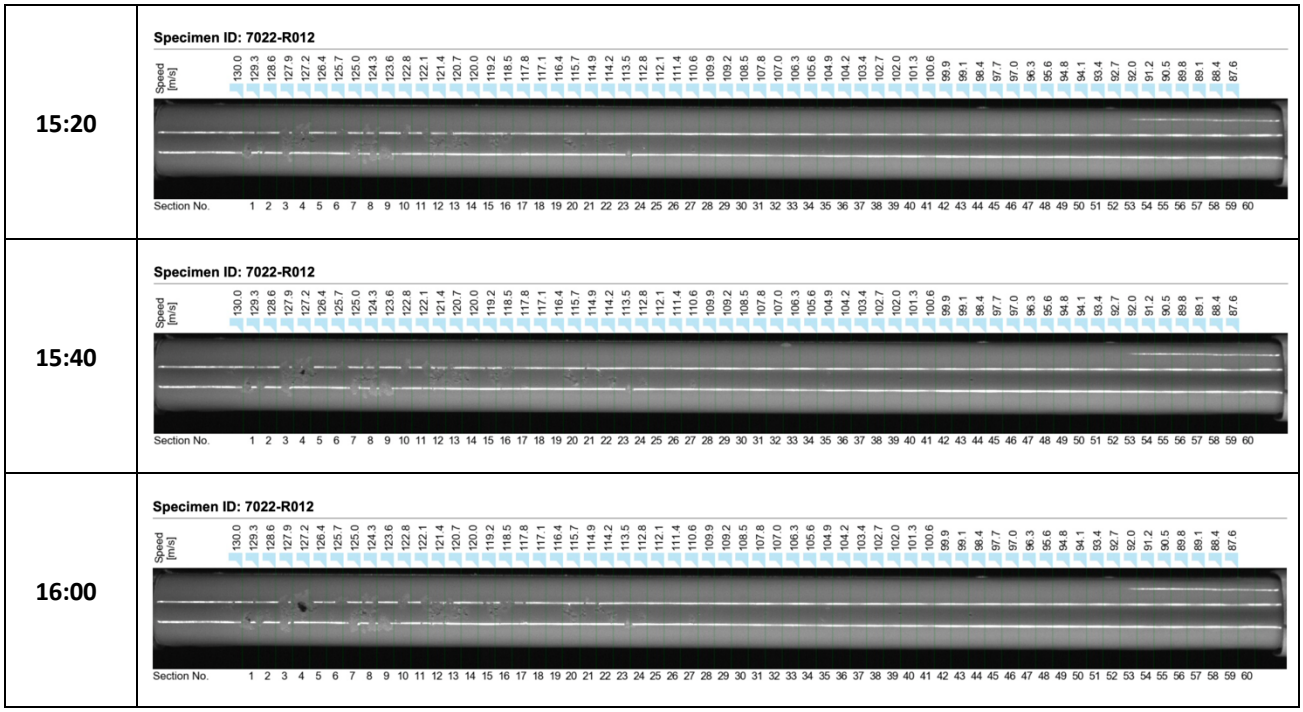

Figure 17. RET testing case for PC with images captured at different time intervals.

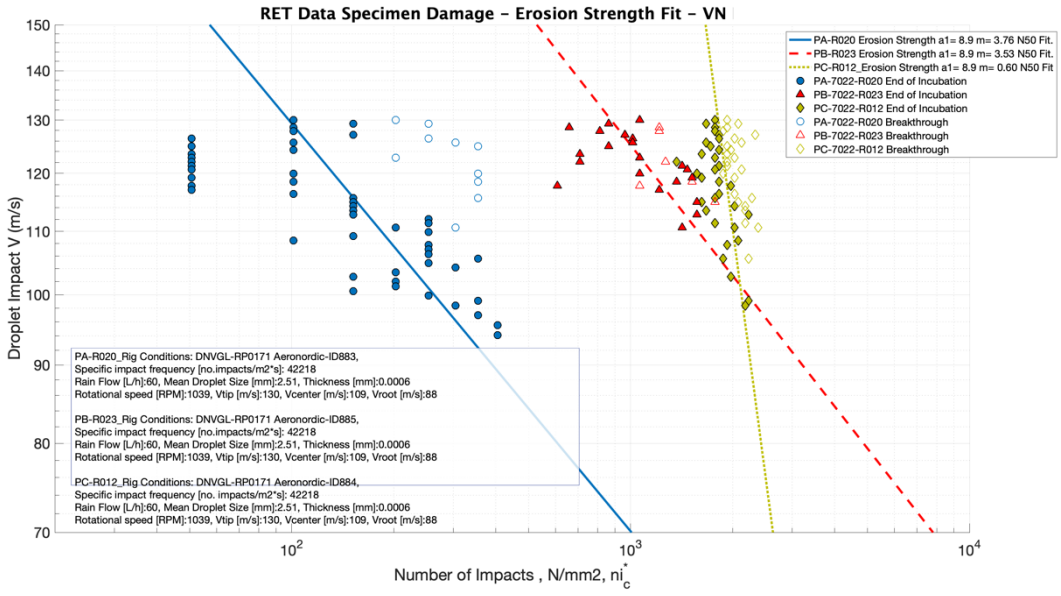

Figure 18. V-N curves of erosion strength for the three compared cases PA, PPB, and PC

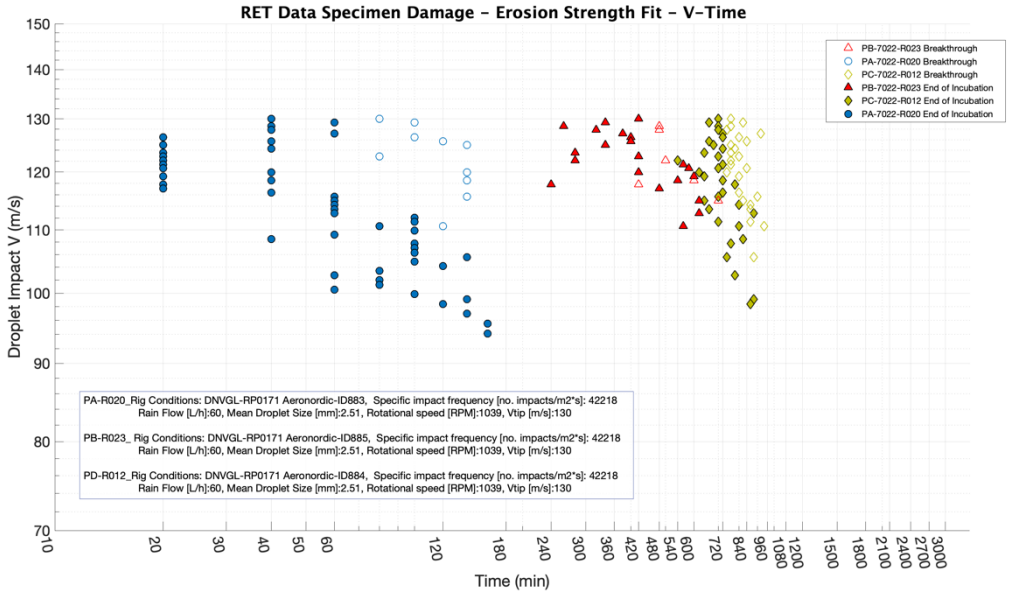

Figure 19. RET Data V-Time exposure and failure mode identification for the three compared cases PA, PB, and PC

Following the incubation period and testing of the breakthrough, the progression of damage can be examined. This study facilitates quantifying the erosion rate more than identifying specific erosion mechanisms outlined in the previous section, and assessing changes in the LEP coating over time due to erosion impact speed relations. The VN curve analysis ploted in Figure 18 show that decreasing number of impacts until failure with the increasing velocity is observed for both PA and PB, while for PC, the slope of the fatigue damage does not depend strongly with the impact speed. A similar pattern with the same number of impacts but the scale of Time instead of the number of impacts is shown in Figure 19. The fitted trend lines of PA and PB are similar ranking PB with better performance. This is coherent with the viscoelastic frequency response shown in Figure 2, and discused previously. In both cases delaminates revealed in Figure 15 and Figure 16 as the main damage mechanism of ersoion. PC case exhibits best durability and performance, as expected from its viscoelastic performance, and also avoids delamination so pitts evolve and grow as craters during exposure time but no interface failure is observed. Neverthles, it is important to note PB and PC intersecting at around v = 100 m/s. When investigating velocities higher than the crossover point, PC experiences a greater number of impacts until the incubation period in comparison to PB. Conversely, at lower impact velocities, PB demonstrates superior performance. Given the relatively mild slope of PB's curve, it is concluded that PB may have longer lifetimes but this test have not been developped so only conclusions due to the VN curves are predicted. This result is coherent with the assumption that at high impact velocities (and therefore frequencies, range 10^4-10^7) the behaviour of PC is considerably higher than PB and also PA.

This result allows one connecting the erosion resistance data with the viscoelastic DMA data in regards the durability of LEP materials comparison within the scope of this research as discussed previously.

3.3 *Case 3. Rain Erosion Testing based on Pulsating Jet Erosion Test (PJET)*

In this section, the methodology employed in the investigation provides a description of the two coatings PA and PB introduced previously and the facilities used to test and observe samples. The test plan for operating the Pulsating Jet Erosion Test (PJET) is outlined first and then, the erosion damage progression analysis is discussed.

A detailed description of the experimental setup and testing methodology has been recently published by the authors in [25]. This study [25] uses the Pulsating Jet Erosion Tester (PJET) to analyze the effects of droplet impact frequencies and dry intervals on damage incubation time in polyurethane-coated samples. A revised PJET approach is proposed to better simulate real-world rainfall, improving predictive models for material degradation. These findings highlight the importance of visco-elastic behavior and intermittent rain in erosion testing, aiding future PJET test designs. Nevertheless, this work compares material performance in different rigs by focusing on damage progression and analysis of damage characteristics, rather than the capabilities of each testing method.

Test setup. Pulsating Jet Erosion Test (PJET)

The two types of coatings, PA and PB, applied on the same filler-substrate layer were used in the experiment. An example of a sample is shown in Figure 20 a. A random selection of PA and PB samples from each batch was measured. The size of the samples was determined using a calliper and found to be 83±5 mm by 81±5 mm. The thickness of each layer was measured using a 3D microscope. The sample was placed on the platform, which was set as the reference height (0 mm). The point height of each layer was then measured, as illustrated in Figure 20 b. By subtracting the point heights, the thickness of each layer was obtained. The coating, filler, and substrate were found to have thicknesses of 0.25±0.09 mm, 0.86±0.05 mm, and 1.22±0.05 mm, respectively.

The test matrix of the sample is shown in Figure 20 c. Each sample provides 16 spots (4 by 4) for each measurement. Every spot is situated at a distance away from one another and the edge in order to eliminate the edge effect and leave sufficient margin for clamping the sample.

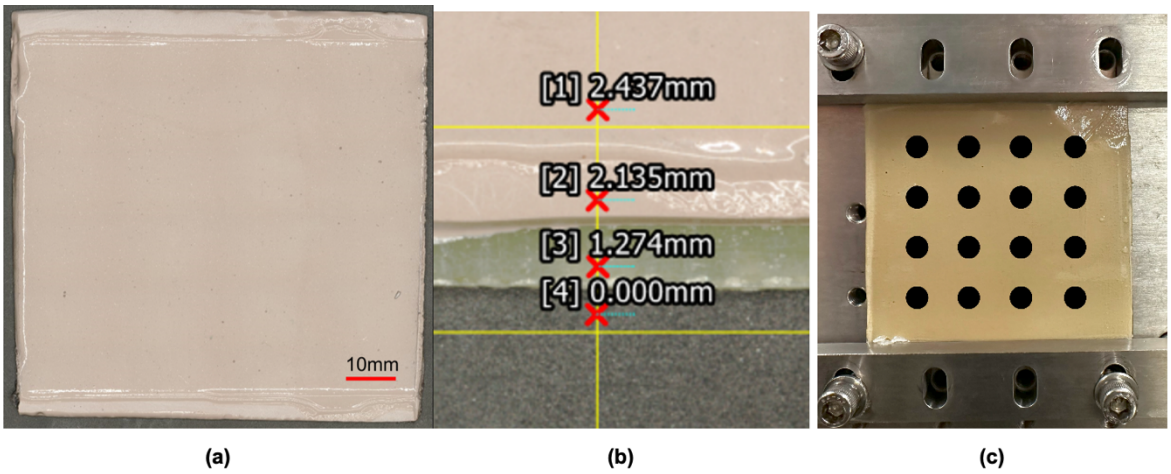

Figure 20. (a) PB sample and (b) its point height of [1] coating, [2] filler, and [3] substrate at a [4] flat surface. (c) Test spots in each sample

To test the performance of the samples under rain erosion, the PJET provided by DUCOM is employed, as shown in Figure 21. Table X shows the designed testing parameters of the facility. The droplet size is determined by the nozzle size and the hole on the disc. For this experiment, a conventional droplet size of 2 mm is chosen. Therefore, the 1.5 mm nozzle is used which is estimated to create droplets with 2 mm diameter due to the expansion resulting from the high pressure. Meanwhile, the diameter of holes on the disc is 2 mm which can constrain the droplet size from expanding beyond 2 mm. The high-pressure pump generates impact velocities ranging from 25 to 250 m/s with an accuracy of ±2 m/s. Impact velocities between 140 and 170 m/s are chosen in this study to strike a balance between testing duration and immediate coating sample destruction. The impact frequency is controllable from 5 to 100 Hz. The air supplier provides 0 to 6 bar pressurized air stream to remove water film avoiding the water cushioning effect. In this experiment, the impact frequency and the pressure of the air supply are set at 42 Hz and 3 bars aligning with the literature

[2630]. The sample is clamped on the sample holder 50 mm away from the nozzle to match the calibration of the velocity. The angle of the sample holder is adjustable between 15 and 90 degrees, but for this experiment, it is fixed at 90 degrees to simulate the most detrimental impact.

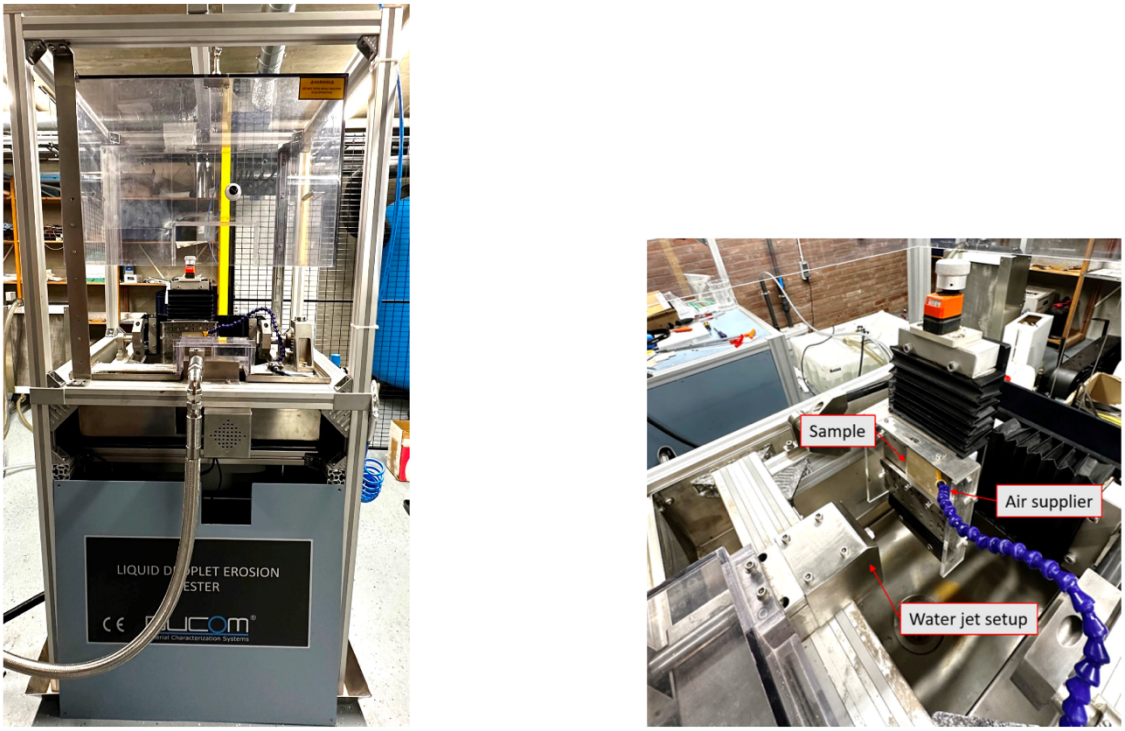

Figure 21. Ducom Liquid Droplet Erosion Tester (b) zoom-in view of components.

Table X. Selected testing parameters for the PJET.

Nozzle size	Impact Velocity	Impact frequency	Air supply	Impact angle
1.5 mm	140-170 m/s	42 Hz	3 bars	90 degrees

[1] Tables may have a footer.

The incubation period and the breakthrough are the two representative moments in erosion since they stand for the first visible fracture on the coating and the first visible penetration of the coating. Therefore, the failure of these two moments is chosen to be tested. The erosion until the incubation period of both PA and PB is performed for three impact velocities: 140, 150, and 160 m/s . Yet, the selected velocities are slightly different in the breakthrough case. We know that the breakthrough is longer than the incubation period. In addition, the experimental results of PA and PB conducted by University of Limerick and described in previous section, show that PB withstands longer against erosion than PA. To fit the time constraint of this study, the lowest impact velocity tested for PA is altered to 145 m/s. A higher range from 150 m/s to 170 m/s is set for PB. Table X displays the number of successful measurements under each condition. The outliers are excluded. The outliers are defined to be not fully damaged in terms of the incubation period and the breakthrough after testing for more than 10 hours and those damage could be observed during operation within 10 minutes.

Table X. Number of successful measurements until the incubation period and the breakthrough for both coating materials at each velocity.

Impact Velocity (m/s)	Incubation		Breakthrough	
	PA	PB	PA	PB
140	2	3	-	-
145			4	
150	4	5	3	5
160	3	3	5	6
170	-	-	-	4

Rain erosion progresion

After the incubation period and the breakthrough are tested, the damage progression in between them can be investigated. This study helps us understand the rate of erosion, better identify the specific erosion mechanisms at play, and examine the changes in the LEP coating over time because of erosion. The experiment is conducted for two intermediate time points. Afterward, the surface damage is evaluated using the microscope. The measured volume is then multiplied by the density of the coating to determine the loss of mass after erosion.

The v − n curve analysis of the test results obtained from the PJET lacks comprehensiveness due to the omission of the volume dependency of impact velocity, impact frequency, and disc geometry. This issue is exemplified in a previous research study [25] where a range of impact frequencies were investigated in relation with the relaxation time for the viscoelastic material to recover and the role of volume (kinetic energy) in erosion. In general, the volume of a water slug produced by a high-speed water jet in the PJET is larger than that of a spherical water droplet with the same diameter. Consequently, the water slug also possesses greater kinetic energy than this moving spherical droplet at the same speed. To compensate for the disregarded variation in volume (kinetic energy) in the v − n curve, while maintaining a conventional representation of impact velocity with respect to the number of impacts, it is proposed the adjusted" equivalent velocity (veq)" based on the consistent reference droplet for the analysis. The concept is to consider, with the reference droplet, how high the equivalent velocity should be to exert the same kinetic energy per impingement as the actual one in the experiment [25]. This implies that for the same size of the droplet at the same equivalent velocity, the higher the impact frequency the fewer the number of droplets needed to cause damage. This observation aligns with the expectation of the recovery of deformation and viscoelastic behavior: as the impact frequency increases, the polyurethane coating has less time to recover from the strain, leading to faster erosion. Overall, using the equivalent velocity to build the plot reduces the water slug volume interdependence with impact velocity and impact frequency when we present the result by velocity-number of impacts relationship.

The outcome of the incubation tests is illustrated by the impact velocity and the equivalent velocity in relation to the number of impacts until the incubation period in Figure 22. The trend of the decreasing number of impacts with the increasing velocity is observed for both PA and PB. The two figures show a similar pattern with the same number of impacts but the scale of veq is higher than that of v. The trend line of PA is steeper than that of PB, intersecting at around v = 151 m/s and veq = 976 m/s . In the investigation of velocities higher than this crossover point, the PA exhibits a greater number of impacts until the incubation period compared to PB. Conversely, at lower impact velocities, PB demonstrates improved performance. Due to the relatively mild steepness of the curve for PB, it is deduced that PB has longer lifetimes for LEP on the comparison with other developed tests in previous sections as the impact velocity is below 150 m/s.

At v = 160 m/s , the average number of impacts until the incubation period of PA and PB is very close and the range of all measurements is narrow. The scatter of the measurements at v = 150 m/s is significant for both materials. The minimum measured number of impacts of PA is nearly the same

as that of the maximum of PB. Yet, their average values are distinct. For the group of v = 150 m/s and v = 160 m/s there is no significant difference in the incubation periods between PA and PB at these velocities. In contrast, a significant variation is found for the impact velocity of 140 m/s. This finding further supports the previous deduction that the incubation period for PB is longer than that for PA as the velocity decreases.

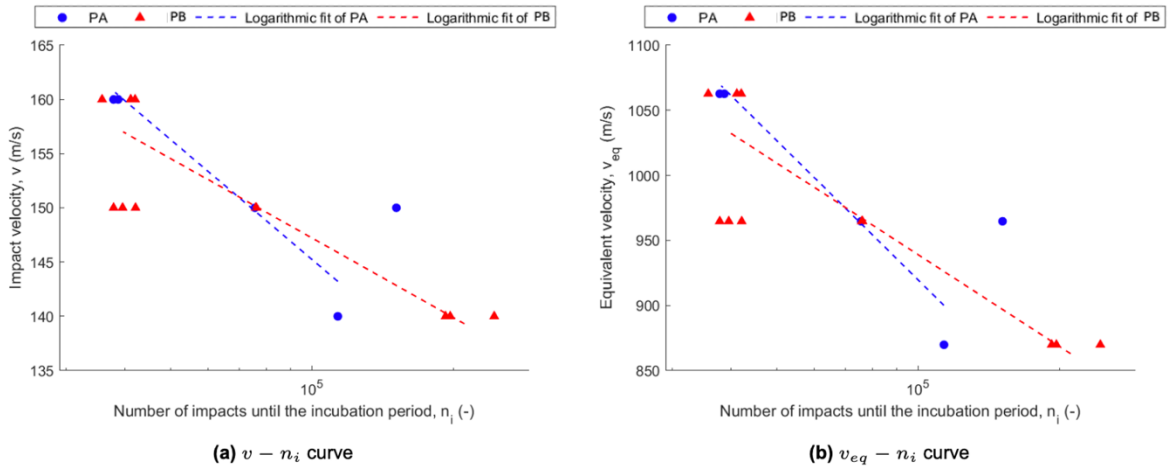

(a) $v - n_i$ **curve** **(b)** $v_{eq} - n_i$ **curve**

Figure 22. Performance of PA and PB presented by the impact velocity and equivalent velocity with respect to the number of impacts until the incubation period.

The erosion durability results from the rain erosion tests align well with viscoelastic response based on DMA testing of Figure 2. The erosion behaviour of these two materials show in Figure 22 that there is a cross-over between the two materials at an impact velocity of 150m/s. At high impact velocities (and therefore frequencies in range of 10^5) the behaviour of PA and PB is similar. At lower impact velocities, PA seems to outperform PB (having a higher tan(δ) in the lower frequency range), after which for a lower impact velocity (140m/s), PB shows the slightly better behaviour in this testing, which can be explained by the consecutive cross-over point in the frequency sweep. Both coatings PA and PB exhibits similar performance at high-speed testing ranges and alternative deductions may be done due to its lowered ability to attenuate energy at high frequencies (10^4-10^7) and the cross-over values in this range. While the delamination effect may contribute to erosion, current adhesion values do not correlate with viscoelastic response; further testing is needed.

The initial damage until the incubation period is investigated via the 3D microscope as shown in Figure 1. It is apparent that the damage for PB is more severe than for PA. The failure mode for PA is mainly pitting. The damage consists of a few dents close by within a circle of 4.5 mm in diameter. The total damaged area is between 0.7 to 1.2 mm^2. The damage characteristic does not vary with three different velocities. On the other hand, relatively large craters can be observed on the surface of PB. The predominant failure mode is cratering. The damaged area tends to grow with increasing velocity. The damaged areas are 5.7, 6.6, and 37.3 mm^2 at 140, 150, and 160 m/s respectively.

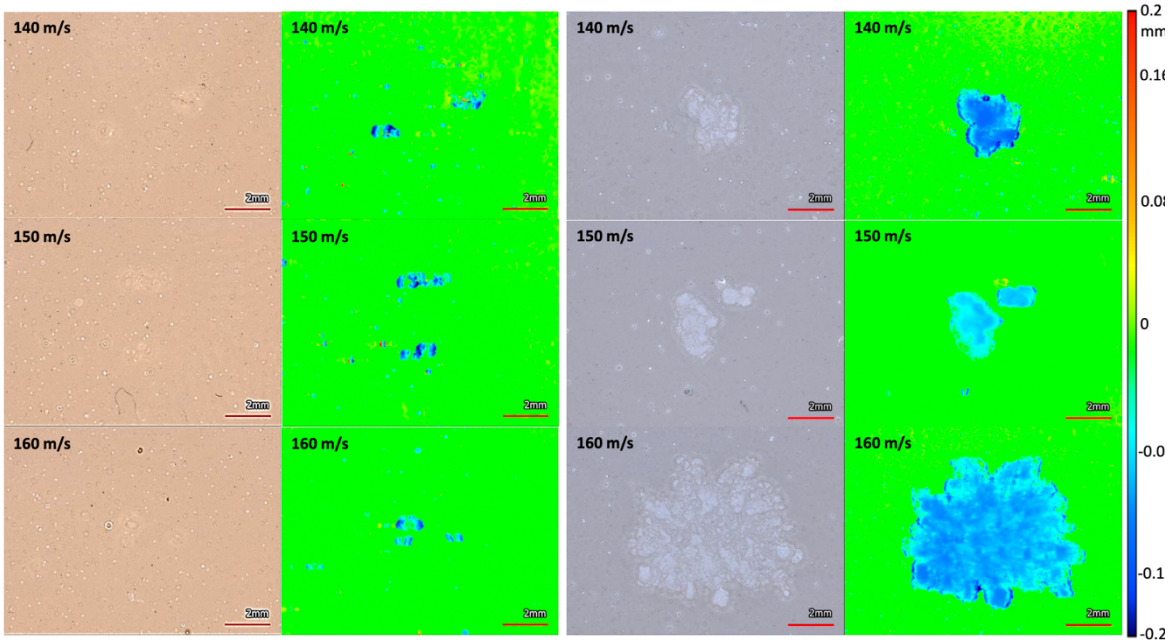

a) PA b)PB

Figure 1. Optical images and height maps showing the surface damage until the incubation period.

After the test for the incubation period, the results of the breakthrough are demonstrated in the section. Figure 2 presents the performance of PA and PB by the erosion test until breakthrough. Like the incubation, the average number of impacts increases as the velocity drops. In Figure 2 PB requires 2 to 3 times more impacts on average than PA to reach the breakthrough at the same velocity. By considering the results of the incubation period in Figure 1Figure 22 and the breakthrough in Figure 2 at the same velocity, it is observed that the erosion time until the breakthrough is 3 to 4 times longer than the incubation period for PA coatings. For PB coatings, the erosion time until the breakthrough is more than 10 times longer than the incubation period.

Besides, the point of intersection does not appear in Figure 2. It would be located at v = 126 m/s and veq = 737 m/s if two curves were extrapolated. Below the point of intersection, the PA demonstrates a greater number of impacts until the breakthrough compared to PB at the same velocity. This implies that the lifetime in terms of the breakthrough is higher for PA than PB undergoing real-life impact velocities. This finding, in conjunction with the results from the incubation test, indicates that PB has a longer incubation period but reaches the breakthrough faster, whereas stiffer materials like PA may offer better resistance against the breakthrough in the low-velocity range. However, further verification under low-velocity testing is required to substantiate these observations.

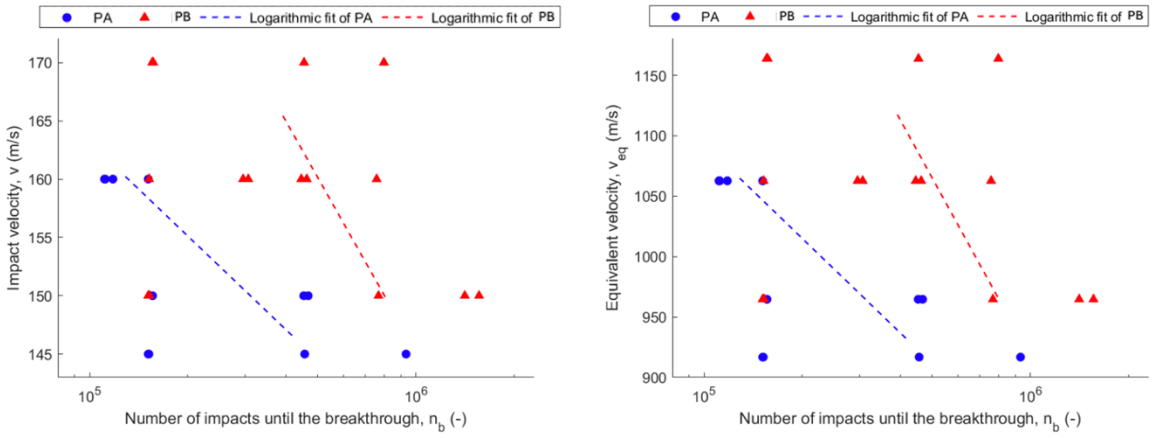

606 **(a)** $v - n_b$ curve **(b)** $v_{eq} - n_b$ curve

607 **Figure 2.** Performance of PA and PB presented by the impact velocity and equivalent velocity
608 with respect to the number of impacts until the breakthrough.

609 The samples were observed after the complete erosion. Figure 3 displays the representative
610 surface damage until the breakthrough at selected impact velocities for PA and PB. All damages until
611 the breakthrough are obvious since the coating layer was penetrated. The main failure mode is pitting
612 for PA and cratering for PB. The damaged areas of PA vary from 4 to 100 mm² regardless of the
613 impact velocity. In contrast, the damaged areas measured among the PB's test spots are more
614 consistent, from 38 to 85 mm². In addition, there are other characteristics found as presented in Figure
615 4. Debonding is seen on several PA surfaces, particularly at high-impact velocities (150 and 160 m/s),
616 and some of them appear with peeling and cracks on the coating. However, these damage
617 characteristics are not seen in PB. Only crater-like damage is observed on the coating but further
618 pitting and cracks on the filler occurred on some test spots. This damage underneath the coating layer
619 is not studied in this research.
620

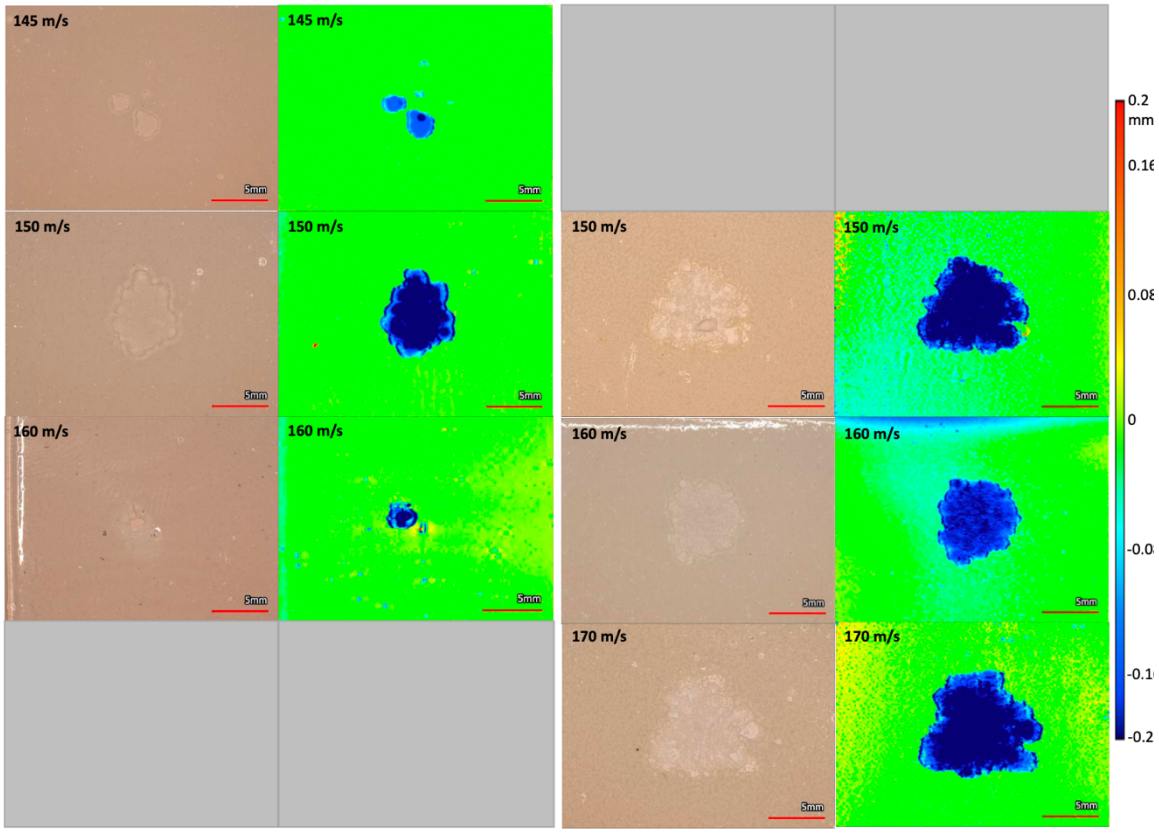

a) PA b) PB

Figure 3. Optical images and height maps showing the surface damage until the breakthrough.

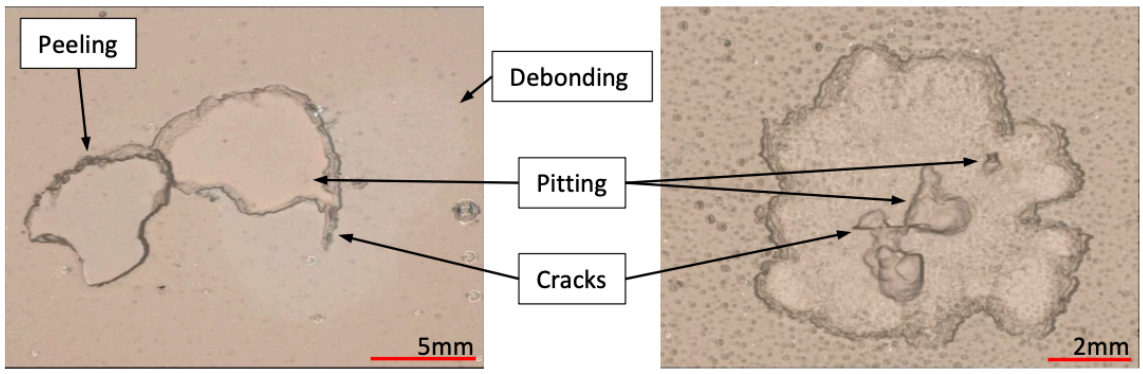

a) b)

Figure 4. Damage characteristics of (a) PA at v =150 m/s and (b) PB at v =170 m/s .

After analyzing the damage progression during the incubation period and breakthrough, we also conducted a few tests in between them to investigate the cumulative erosion process for both PA and PB coatings. These tests were performed at an impact velocity of 160 m/s, which corresponds to the available data for incubation and breakthrough. Their results are presented in Figure 5 which depicts the erosion graph illustrating the progression of mass loss over the testing duration and damaged area over the testing duration. Examples of microscopic surface erosion corresponding to each testing interval are shown in Figure 6.

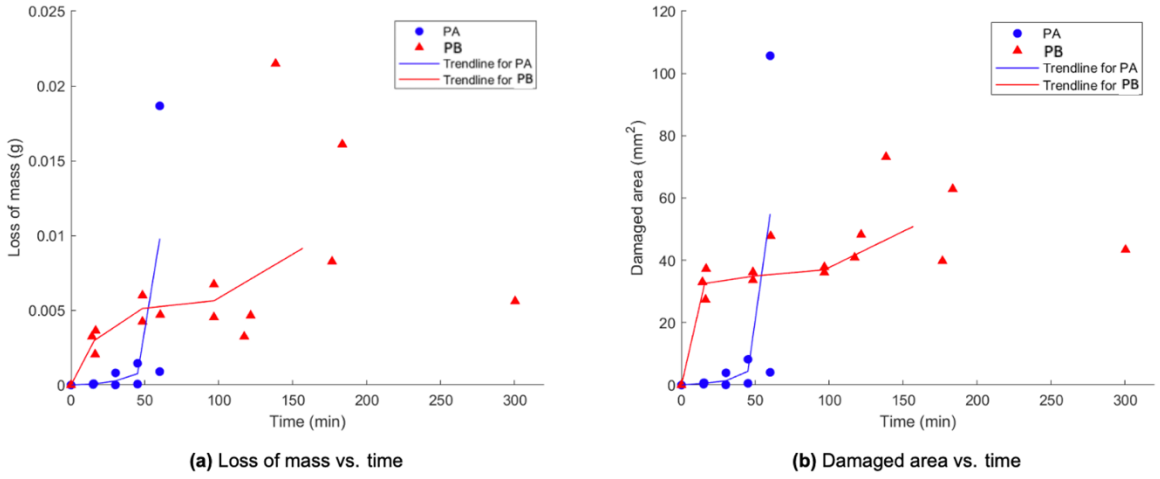

Figure 5. Erosion graph until the breakthrough of PA and PB at v = 160 ms .

The erosion progression observed for PA and PB coatings exhibit distinct characteristics in Figure 5. For PA, shown in Figure 17a, mild damage occurs within a short time span of 50 minutes, followed by a significant increase in the average mass loss from less than 0.001 to nearly 0.01 grams in the subsequent 15 minutes, corresponding to the breakthrough. This phenomenon can also be observed from Figure 17a, where the surface damage starts with mild pitting, advances to gouges, and eventually leads to an obvious loss of material and debonding until the breakthrough. The trend for the damaged area over the erosion time of PA in Figure 17b, is similar to its mass loss progression in Figure 17a, implying the growth of damage is attributed to both the thickness and area.

On the other hand, PB demonstrates a more gradual mass loss throughout the entire erosion progression in Figure 17a. Nevertheless, the size of the damaged area tends to stabilize at around 45 mm^2 after the incubation period as shown in Figure 6b. This trend is also evident in Figure 6b, where a substantial crater is observed initially and its size remains relatively unchanged until the breakthrough. Hence, it highlights that the growth of damage in PB is mostly through thickness after the initial damage appears.

The total mass losses until the breakthrough are approximately the same (0.01 grams) for both PA and PB coatings although the damaged topography differs between the two. Despite the fact that the damaged area of PB is greater than that of PA, as evident from the darkest blue region in the height map, the extent of PB eroded down to the filler material is tiny, whereas a considerably larger area of PA has eroded to the filler.

In the aspect of surface morphology, PA exhibits higher mass loss per unit area compared to PB. This may imply that the erosion mechanisms of the two materials differ. Based on the observed large area of damage, it is reasonable to deduce that lateral jetting plays a significant role in the erosion of PB. This can be attributed to its low Young's modulus, which allows water to deform the material and pave the way for lateral jetting. In contrast, the stiff property of PA results in pitting characteristics on its sur- face, which may be caused by the water hammer pressure and stress waves rather than lateral jetting. The damage in PA seems to mainly occur in localized areas, while the surrounding material remains relatively undisturbed. Over time, the pits on PA's surface grow and merge, leading to a larger area of damage until the breakthrough. However, only the failures that involve debonding and peeling, as shown in Figure 4a demonstrate the evident influence of lateral jetting. Additionally, the ductile nature of PB contributes to a more gradual loss of mass during the erosion process. The material's ability to dissipate the impact over a broader region helps reduce the severity of damage in any single localized area. From the experimental point of view, Young's

modulus might be a key factor in the erosion resistance as the other properties of PA and PB are quite similar.

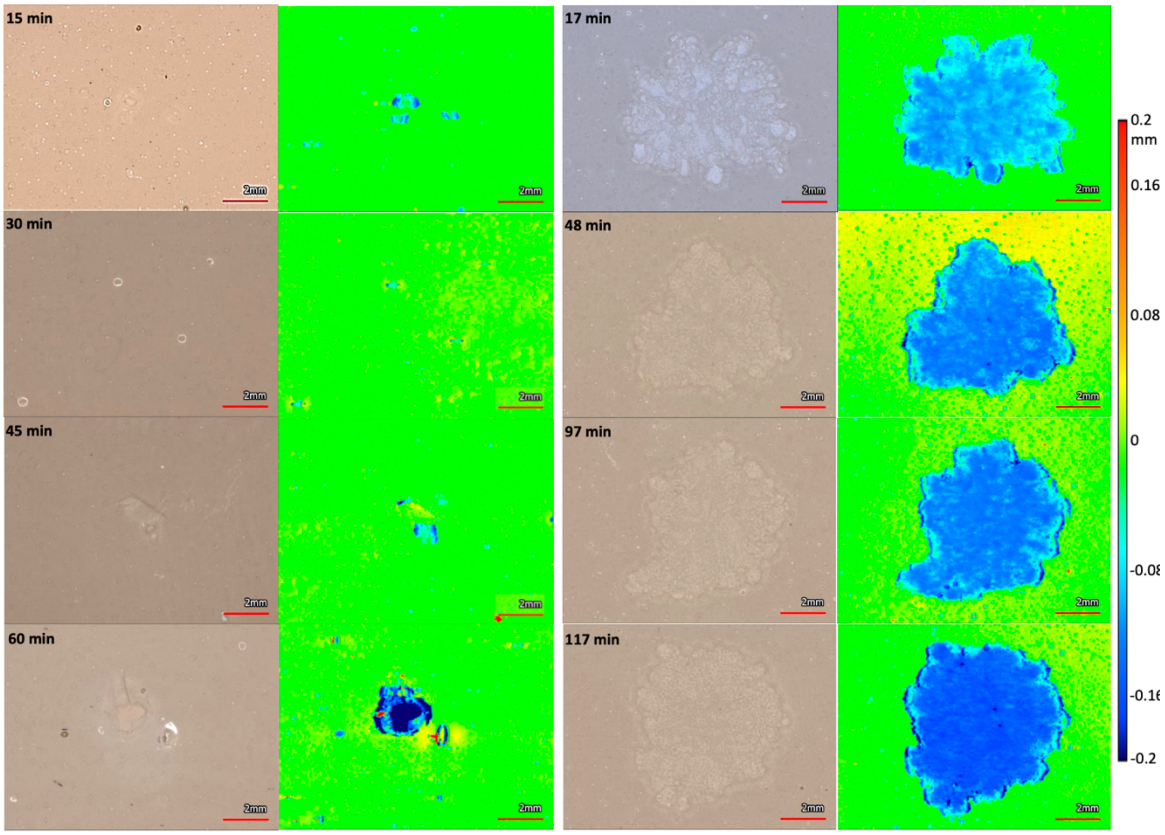

a) PA b) PB

Figure 6. Microscopic images of mass loss progression of (a) PA and (b) PB at v = 160 ms . Images from top to bottom show progressive surface erosion from the incubation period to the breakthrough.

Conclusions

The investigation has analyzed erosion damage progression tesing experiments to connect mechanical behavior with polymer properties and microstructure of candidate coatings. Different rain erosion testing methods are compared, including whirling arm rigs and a pulsating water jet tester, to assess lab performance for various LEP chemistries. Material characterization used dynamic mechanical analysis to observe visco-elastic behavior. Damage was examined through CT scanning to provide data for failure mode analysis.

Similar failure modes and durability rankings for each LEP material comparison were observed in the different RET testing methodologies.

In regards quantifying the erosion rate results showed that the durability of the materials described by the mass loss plots or the VN slopes depend strongly with the impact speeds. Moreover, the viscoelastic frequency response of the materials allows one connecting the erosion resistance data with the viscoelastic DMA data in regards the durability and erosion progresion of the LEP materials. The case that exhibits best erosion durability and performance, coating PC, is the one that improves its impact energy attenuation capabilities at at high impact velocities (and therefore frequencies,

range 10^4-10^7). The behaviour of coating PC is considerably higher than PB and also PA due to its viscoelastic performance, but also with the same argument this material can be worse at lower impact velocities. These results point out the substantial dependence of testing results due to viscoelastic material performance. Dynamic mechanical analysis showed that LEPs switch between high or low capabilities to attenuate impact energy or elastic and brittle failure modes at a critical impact frequency. Testing impact speed configurations may provoque dissimilar LEP performance depending on the viscoelastic response of the materials.

This result allows one connecting the erosion resistance data with the viscoelastic DMA data in regards the durability of LEP materials comparison within the scope of this research as discussed previously. Additional research is needed to relate delamination issues at interface due to the lack of such viscoelastic effects.

Funding

This research was supported by the project "SISTEMA DE PROTECCIÓN DEL BORDE DE ATAQUE DE LAS PALAS DE AEROGENERADOR BASADO EN MATERIA PRIMA DE ORIGEN RENOVABLE-RENEWEDGE", reference INNEST/2024/47, funded by the program "Proyectos Estratégicos en Cooperación", Valencian Innovation Agency (AVI), Generalitat Valenciana, Spain. Financial support was provided by the Sustainable Energy Authority of Ireland (SAEI) under grant RDD671.

Acknowledgments

The authors would also like to thank the International Energy Agency (IEA) Wind TCP Task 46 (Erosion of Wind Turbine Blades) for creating an environment for research collaboration.

References

1. Analyzing rain erosion using a Pulsating Jet Erosion Tester (PJET): Effect of droplet impact frequencies and dry intervals on incubation times, AS Verma, CY Wu, MA Díaz, JJE Teuwen - Wear, 2025
2. Dunson, Characterization of polymers using dynamic mechanical analysis (dma), EAG Appl Note (2017).
3. I. Ouachan, M. Kuball, D. Liu, K. Dyer, C. Ward, I. Hamerton, Understanding of leading edge protection performance using nano-silicates for modification, in: Journal of Physics: Conference Series, Vol. 1222, IOP Publishing, 2019, p. 012016.
4. https://www.tainstruments.com/wp-content/uploads/Boston-DMA-Training-2019.pdf
5. Young RJ, Lovell PA. Introduction to Polymers. 3rd ed. CRC Press; 2011.
6. ABAQUS 2024 Documentation. Viscoelasticity: Guide Theory. Mechanical Constitutive Theories. Dassault Systèmes.
7. ASTM. ASTM G73-10 "Standard Test Method for Liquid Impingement Erosion Using Rotating Apparatus"; ASTM: West Conshohocken, PA, USA, 2013.
8. Busch, H.; Hoff, G.; Langbein, G.; Taylor, G.; Jenkins, D.C.; Taunton, M.A. Rain erosion properties of materials and discussion. Philos. Trans. R. Lond. A 1966, 260, 168–81.
9. Castorrini, A., Barnabei, V., Domenech, L., Sakalyte, A., Sánchez, F. Campobasso, M.. Impact of meteorological data factors and material characterization method on the predictions of leading edge erosion of wind turbine blades, Renewable Energy, 2024, 227, 120549
10. DNVGL-RP-0573. Evaluation of Erosion and Delamination for Leading Edge Protection Systems of Rotor Blades, DNV GL, Oslo, Norway, 2020.
11. DNVGL-RP-0171, Testing of Rotor Blade Erosion Protection Systems, Recommended practice, DNV GL, Oslo, Norway (2018).

12. Domenech, L., Renau, J., Sakalyte, A. and Sanchez, F.. Top coating anti-erosion performance analysis in wind turbine bladese depending on relative acoustic impedance. Part 1: Modelling Approach. Coatings, 10, 685, 2020.
13. Eisenberg, D.; Laustsen, S.; Stege, J. Wind turbine blade coating leading edge rain erosion model: Development and validation. Wind Energy 2018, 21, 942–951, doi:10.1002/we.2200.
14. Hao, Hao and Domenech, Luis and Sánchez, Fernando, Modeling Rain Erosion Surface Damage Initiation in Turbine Blades Based on Inspection Data at Wind Farms (December 18, 2024). Available at http://dx.doi.org/10.2139/ssrn.5062754
15. Herring, R., Domenech, L., Renau, J., Sakalyte, A., Ward, C., Dyer, K. and Sanchez, F.. Assessment of a wind turbine blade erosion lifetime prediction model with industrial protection materials and testing methods. Coatings, 11, 767, 2021.
16. O'Carroll A., Hardiman M., Tobin E.F., Young T.M., Correlation of the rain erosion performance of polymers to mechanical and surface properties measured using nanoindentation, Wear, 412-413 (2018) 38-48.
17. Prieto, R., Karlsson, T. A model to estimate the effect of variables causing erosion in wind turbine blades. Wind Energy, 2021, 24 (9), 1031–1044.
18. Pryor, S., Barthelmie, R., Cadence, J., Dellwik, E., Hasager, C., Kral, S., Reuder, J., Rodgers, M., Veraart, M.. Atmospheric Drivers of Wind Turbine Blade Leading Edge Erosion: Review and Recommendations for Future Research. Energies, 2022, 15, 8553
19. Pryor, S.C.; Coburn, J.J.; Barthelmie, R.J. Spatiotemporal Variability in Wind Turbine Blade Leading Edge Erosion. Energies 2025, 18, 425. https://doi.org/10.3390/en18020425
20. Springer, G.S. Erosion by Liquid Impact; Scripta Technica Publishing Co.: Washington, DC, USA, 1976.
21. Springer, G.S.; Lang, C.-I.; Larsen, P.S. Analysis of Rain Erosion of Coated Materials. J. Compos. Mater. 1974, 8, 229.
22. Slot, H. M., Gelinck, E. R. M., Rentrop, C., van der Heide, E.. Leading edge erosion of coated wind turbine blades: Review of coating life models. Renewable Energy, 2015, 80, 837-848
23. Tobin, E.; Young, T.; Raps, D.; Rohr, O. Comparison of liquid impingement results from whirling arm and water-jet rain erosion test facilities. Wear 2011, 271, 2625–2631, doi:10.1016/j.wear.2011.02.023.
24. Verma, A.S.; Noi, S.D.; Ren, Z.; Jiang, Z.; Teuwen, J.J.E. Minimum Leading Edge Protection Application Length to Combat Rain-Induced Erosion of Wind Turbine Blades. Energies 2021, 14, 1629. https://doi.org/10.3390/en14061629.
25. Verma A., Wu C., Díaz M.A., Teuwen, J. Analyzing rain erosion using a Pulsating Jet Erosion Tester (PJET): Effect of droplet impact frequencies and dry intervals on incubation times, Wear, 2025, 205614, 562–563
26. Zhiwei Wu, Nezam Azizaddini, Claus Erik Weinell, Kim Dam-Johansen, Søren Kiil, Characterization of a pulsating water jet for rain erosion testing of blade coatings: Flow visualization, pressure investigation, and damage analysis, Materials Today Communications, Volume 40, 2024, 109898, ISSN 2352-4928, https://doi.org/10.1016/j.mtcomm.2024.109898.
27. Donnell, L.. Longitudinal wave transmission and impact. American Society of Mechanical Engineers, 52, 153-167, 1930.
28. Domenech, L., Renau, J., Sakalyte, A. and Sanchez, F.. Top coating anti-erosion performance analysis in wind turbine bladese depending on relative acoustic impedance. Part 1: Modelling Approach. Coatings, 10, 685, 2020.
29. Bech, J., Johansen, N., Madsen, M., Hannesdottir, A. and Hasager, C.. Experimental study on the effect of drop size in rain erosion test and on lifetime prediction of wind turbine blades. Renewable Energy, 197, 776-789, 2022.
30. ASTM E739-10(2015). Standard Practice for Statistical Analysis of Linear or Linearized Stress-Life (S-N) and Strain-Life (ε-N) Fatigue Data, ASTM International, West Conshohocken, PA, USA, 2020.
31. Best, A.. The size distribution of raindrops. Quarterly Journal of the Royal Meteorological Society, 76(327), 16-36, 1950.
32. www.aero-nordic.com/test-type/rain-erosion-test (accessed February 2025).
33. Kinsley, P.; Porteous, S.; Jones, S.; Subramanian, P.; Campo, O.; Dyer, K. Limitations of Standard Rain Erosion Tests for Wind Turbine Leading Edge Protection Evaluation. Wind2025,5,3. https://doi.org/10.3390/wind5010003

34. Akindoyo, J. O., Beg, M. D. H., Ghazali, S., Islam, M. R., Jeyaratnam, N., & Yuvaraj, A. R. (2016). Polyurethane types, synthesis and applications – a review. RSC Advances, 6(115), 114453–114482. https://doi.org/10.1039/C6RA14525F
35. Zoran S. Petrović, James Ferguson,Polyurethane elastomers, Progress in Polymer Science, Volume 16, Issue 5, 1991, Pages 695-836,ISSN 0079-6700, https://doi.org/10.1016/0079-6700(91)90011-9.
36. L.Mishnaevsky,S.Fæster,L.P.Mikkelsen,Y.Kusano,J.I.Bech,Micromechanismsofleadingedgeerosionofwind turbineblades:X–ray tomography analysis and computational studies, Wind Energy 23 (3) (2020) 547–562. doi:10.1002/we.2441.
37. Cortés, E.; Sánchez, F.; O'Carroll, A.; Madramany, B.; Hardiman, M.; Young, T.M. On the material characterization of wind turbine blade coatings: Effect of the interphase adhesion on rain erosion performance. *Materials* **2017**, *10*, 1146.
38. Fernando Sánchez, Aurelio Olivares, Luis Domenech and Enrique Cortés. A numerical modelling approach for interphase adhesion of rain erosion protection systems of wind turbine blades.. Proceedings of ECCM18 - 18th European Conference on Composite Materials.